

# THE PROPERTIES OF X-RAY AND OPTICAL LIGHT CURVES OF X-RAY NOVAE

Wan Chen<sup>1,2</sup>, C. R. Shrader<sup>1,3</sup>, and Mario Livio<sup>4</sup>

<sup>1</sup> Laboratory for High Energy Astrophysics, NASA/Goddard Space Flight Center, Greenbelt, MD 20771

<sup>2</sup> Department of Astronomy, University of Maryland, College Park, MD 20742

<sup>3</sup> Universities Space Research Association

<sup>4</sup> Space Telescope Science Institute, 3700 San Martin Drive, Baltimore, MD 21218  
chen@milkyway.gsfc.nasa.gov, shrader@grossc.gsfc.nasa.gov, mlivio@stsci.edu

(Accepted on 10 July 1997 for publication in the *Astrophysical Journal*, Part 1)

## ABSTRACT

We have collected the available data from the literature and from public data archives covering the past two decades for the long-term X-ray and optical light curves of X-ray nova (XN) outbursts. XN outbursts are due to episodic accretion events, primarily in low-mass X-ray binaries normally characterized by low mass transfer rates. Dynamical studies indicate that most XNs contain a black hole. The soft X-ray emission during outburst traces the accretion rate through the inner edge of the accretion disk, while the optical light curve traces the physical conditions at the outer disk – thus collectively they contain information on the time-dependent behavior of accretion processes through the disks.

In this paper we carry out for the first time a systematic, statistical study of XN light curves which are classified into 5 morphological types. Basic light curve parameters, such as the outburst peak flux, amplitude, luminosity, rise and decay timescales, the observed and expected outburst durations, and total energy radiated, are tabulated and discussed. We find that the rise timescales have a flat distribution while the decay timescales have a much narrower and near-Gaussian distribution, centered around 30 days and dominated by the strongest outbursts. The peak luminosity is also distributed like a Gaussian, centered around 0.2 in Eddington units, while the total energy released has a much broader distribution around  $10^{44}$  ergs. We find no intrinsic difference between black hole and neutron star systems in their distribution of peak amplitudes.

We identify and discuss additional light curve features, such as precursors, plateaus, and secondary maxima. The plateaus exhibited in the light curves of black hole sources are found to have, on average, longer durations and they are followed by longer decays. The identified secondary maxima seem to occur mostly in black hole systems. For the frequency of outbursts, we find that the average XN outburst rate is about 2.6 per year for events  $> 0.3$  Crab, and that the mean recurrence time between outbursts from a single source is 6 years. The spatial and  $\log(N) - \log(S)$  distribution of the XN sources, with limited statistics, agrees with a source population in the Galactic disk, as observed from a point at a distance of 8.5 kpc from the Galactic center. Finally, we point out that the observed XN light curve properties can in general be explained by a disk thermal instability model, although some important problems still remain.

Keywords: X-rays; stars; black holes; accretion disks

## 1. INTRODUCTION

On 4 April 1967 an X-ray rocket experiment detected a new X-ray source almost as bright as Sco X-1 in the 2–5 keV range (Harries et al. 1967). The new source, Cen XR-2, was not detected on 28 October 1965 (Grader et al. 1966), thus indicating a flux increase by a factor of  $> 100$  during 1967. This was unprecedented among about a dozen known X-ray sources at the time. A series of follow-up rocket flights found that the X-ray flux of Cen X-2 peaked on April 10, then declined *exponentially* with an e-folding time of  $\sim 30.5$  days, disappearing by late September. This behavior led its discoverers to name Cen X-2 an *X-ray nova*, i.e., a transient X-ray source with a light curve analogous to that of a classical nova in the optical (Chodil et al. 1968).

In the 1970’s and early 1980’s, many bright X-ray transient events were discovered by scanning instruments or all-sky monitors (ASMs) aboard the *UHURU*, *Vela*, *Ariel 5*, *OSO 7*, and *Hakucho* satellites, and also by the pointing instruments on the *Ariel 5*, *SAS-3*, *HEAO-1*, and *EXOSAT* satellites. These transients were classified according to their distinctive X-ray spectral properties near the peak of the outbursts (e.g., White, Kaluziński, & Swank 1984 and references therein). Sources with a characteristic bremsstrahlung temperature  $kT_b < 15$  keV were called soft X-ray transients (SXTs) while sources with  $kT_b > 15$  keV were called hard X-ray transients (HXTs).

The HXTs were later found to be Be binary pulsars in highly eccentric orbits with periods of a few weeks to a few months (e.g., Maraschi, Treves, & van den Heuvel 1976). An X-ray outburst may occur in these systems when the neutron star (NS) comes close to the Be star and plunges into its highly flattened dense wind. Because Be star winds are episodic, not every periastron passage involves an outburst. The HXTs usually display a light curve roughly symmetric in the rise and decay phases.

The SXTs, on the other hand, occur in low-mass X-ray binaries (LMXBs), in which a Roche-lobe overflowing, main-sequence or subgiant star of typically  $< 1 M_\odot$  orbits a NS or a black hole (BH), with an orbital period of a few hours to a few days. SXTs undergo episodic X-ray and optical outbursts with light curves similar to that of the first X-ray nova Cen X-2, and they are the subject of this paper. Several SXTs exhibit Type-I X-ray bursts, but no pulsations have ever been detected. About  $\sim 50\%$  of the SXTs were called “ultra-soft” (White, Kaluziński, & Swank 1984), due to the fact that in their peak, a soft excess of  $kT_{\text{brem}} \lesssim$  a few keV has been observed on top of a power-law hard tail. The spectra usually harden as the flux decreases. This property is reminiscent of the bi-modal spectral behavior of BH candidates (BHCs) such as Cyg X-1, and thus suggests a possible high incidence of BH primaries in SXTs.

The terms *X-ray novae* and *soft X-ray transients* have been used interchangeably in the literature. Several recent events (e.g., GRS 1716–249, GS 2023+338, and GRO J0422+32), however, showed pure power-law spectra without the soft excess, while having low mass companions and displaying light curves similar to other SXTs. They are not SXTs in the traditional sense but belong to the SXT family. For clarity, we use the term X-ray nova (XN) throughout this paper.<sup>1</sup>

XNs offer a significant advantage over persistent LMXBs in terms of the potential to perform dynamical studies of the binary system. After the outburst, an XN eventually returns to a quiescent state with its optical light dominated by the secondary star, thus allowing for detailed photometry and spectroscopy to

---

<sup>1</sup>One should not confuse XNs with classical novae in which the accreting object is a white dwarf. For example, the name “Nova Oph 1993” has been attributed to both X-ray Nova GRS 1716–249 and a classical nova which occurred in the same year. We suggest that such X-ray transients should always be referred to as an *X-ray nova*, e.g., “X-ray Nova Ophiuchi 1993” or “XN Oph 1993”.

determine the system parameters of the binary, notably the mass function. XN 0620–00 (XN Mon 1975) was the first low-mass binary proven in this manner to contain a compact object of mass definitively greater than  $3 M_{\odot}$  (McClintock & Remillard 1986), the widely accepted mass upper limit for a stable NS. Thus, XN 0620–00 may contain a BH (see also Haswell et al. 1993; Shahbaz, Naylor, & Charles 1994).

Since 1988, the ASMs on the *Ginga* and *GRANAT* satellites and on the *Mir-Kvant* space station, and the BATSE instrument on the *Compton Gamma Ray Observatory* have been detecting bright XNs at a rate of 1–2 per year. Many of them have subsequently been studied in great detail both in X-rays and in the UV, optical, and radio wavelengths. Remarkable progress has been achieved in identifying 7 sources as BHCs on the basis of orbital dynamical studies (Table 1; see also White & van Paradijs 1996). Five of these are sources discovered since the *Ginga* mission was flown. Currently, the majority of the XNs are classified as BHCs, at least on the basis of their X-ray spectral properties (White 1994; Cowley 1992; Tanaka & Lewin 1995). XNs are thus ideal sources for the study of accretion disks around BHs over a large range of accretion rates, and for studying the formation and evolution of high mass-ratio BH binary systems.

A review of historical XNs was presented in van Paradijs & Verbunt (1984), and their spectral properties were summarized by White, Kaluzienski, & Swank (1984). A catalog of 34 X-ray transients, including 17 XNs, was compiled by Amnuel & Guseinov (1979). Owing to the improved all-sky coverage since the late 1980’s, the number of cataloged XNs has by now more than doubled. In the recent catalog of X-ray binaries (van Paradijs 1995, hereafter vP95), 41 transients were included among 124 LMXBs. A few additional sources have recently appeared (see Tanaka & Shibazaki (1996) and Tanaka & Lewin (1995) for recent reviews). Some of the fundamental outburst properties reported previously are by now well established, and more detailed features of the XN light curves and spectra have emerged. This trend is likely to continue, in light of the recently launched *Rossi X-ray Timing Explorer (RXTE)*. In the meantime, substantial progress has been made in our understanding of the physical mechanisms involved (e.g., Cannizzo, Chen, & Livio 1995 and references therein; Narayan, Barret, & McClintock 1997; Narayan 1997 and references therein). This seems, therefore, to be an appropriate time for a systematic study of all the known XNs and the properties of their light curves using all the data available, as we attempt in this paper.

The paper is organized as follows. In § 2 we discuss the source selection criteria, the methods and scope of our data collection, and the procedures we followed to present the data in a uniform manner. In § 3 we discuss general light curve morphologies and identify different types of light curve shapes and features. Before going into details of the light curves, in § 4 we discuss the properties of quiescent emission of the XN sources. In § 5 we present our analysis of the light curve properties, including the basic parameters which can be defined for almost all the X-ray and optical light curves (§ 5.1), and several features which are seen only in a subset of the light curves, but which are nevertheless of interest and importance towards a complete understanding of the XN phenomenon (§ 5.2). In § 6 we discuss the frequency of XN outbursts, recurrence times, the spatial distribution, and population of XN sources in the Galaxy. In § 7 we touch briefly on the applicability of several broad classes of theoretical models. A summary and conclusions follow in § 8.

## 2. SOURCE AND DATA COLLECTION

## 2.1. Source Selection

In the literature, the name transient is loosely applied to a wide range of phenomena, including X-ray and  $\gamma$ -ray bursters which may or may not show detectable fluxes outside the bursting periods, which are usually a few seconds to a few minutes long (Woosley 1984). To study X-ray transients which have intrinsically similar *long-term* X-ray temporal behavior, we define an XN to be a source which satisfies at least 4 of the following 5 conditions:

- (1) The source had at least one X-ray outburst lasting more than 10 days;
- (2) It is not identified with a Be HXT;
- (3) Its X-ray light curve has the typical fast-rise and exponential-decay profile;
- (4) Its highest peak X-ray flux is at least a factor of 10 higher than its quiescent flux;
- (5) Its quiescent phase lasts at least 10 times longer than the outburst phase.

In Table 2 we list all the sources we have identified so far under these criteria.

Our sample of 24 sources includes 21 of the 41 low-mass transients listed in the vP95 catalog, for which the data collection ended in December 1992, and three new XNs: GRS 1009–45, GRO J1655–40, and GRS 1716–249. Of the 20 low-mass X-ray transients listed as possible XNs (Table 3), Cir X-1 is probably a high-mass X-ray binary with high and low states similar to Cyg X-1 (Moneti 1992). MX 1730–335 is the Rapid Burster, for which large flux variations are probably caused by type I and type II bursts (Grindlay & Gursky 1977). The remaining 18 sources, many of which are located in the crowded Galactic center region, are of unclear transient nature.

It may be difficult to distinguish an XN from an extremely variable but persistent source. Certain sources may straddle a stability line which depends on the amount of X-ray irradiation of the disk – above it the system will be stabilized (van Paradijs 1996). For example, 4U 1608–522 is classified as an XN in the literature, but it has exhibited fairly high flux levels between many moderate-amplitude outbursts (Lochner & Roussel-Dupré 1994), and it is sometimes called a persistent X-ray source. On the other hand, the BHC GX 339–4 is listed as a transient in vP95, but is often regarded as a persistent, highly variable source possessing three distinctive (high, low, and off) intensity states (e.g., Markert et al. 1973; Tanaka & Lewin 1995). We included 4U 1608–522 in our sample and GX 339–4 in our list of possible sources, but we note that they may belong to the same subclass located in the transition region between XN and persistent sources.

Table 4 lists some general information for known XNs (hereafter we will refer to a source by its celestial coordinates name, such as XN 0620–00 or simply XN 0620). Among the 24 XN sources, there are 7 dynamically confirmed and 10 X-ray spectroscopic BHCs (71%) and 7 NS (basically all those not considered to be BHCs); 19 (80%) sources are optically identified but only 9 (37%) of them have the companion star and orbital information available. For 19 (80%) XN sources we have distance estimates from either the X-ray absorption column or optical measurements.

## 2.2. Light Curve Database

For the 24 XNs in our sample, there are 66 recorded outbursts. For 49 of the outbursts, we have collected a total of 58 X-ray and 10 optical light curves, including light curves of the same outburst in different energy bands. Most of these light curves are taken from the literature by digitizing the published light curve plots. Some light curves were kindly provided by the original observers. We have searched the IAU circulars from the late 1960’s up to the present and the *Ariel 5*, *Vela 5B*, *Ginga*, and *UHURU* databases at the High Energy Astrophysics Science Archive Research Center (HEASARC) for information on additional, weak outbursts and data points that complement the published light curves.

The XN light curves were reported in a variety of time units such as the calendar date, the Julian date, days of the outburst year, or days after the outburst. X-ray fluxes were also reported in a variety of units such as instrument count rates, UHURU flux units (UFU), energy flux ( $\text{ergs s}^{-1} \text{cm}^{-2}$ ), photon flux ( $\text{photons s}^{-1} \text{cm}^{-2}$ ), or Crab units. The last case is particularly useful in that it allows a comparison of source brightnesses despite the lack of precise knowledge regarding spectral and instrument response properties. Still, the quantitative comparisons we conduct in this paper will be limited in their precision by the absence of reliable instrument cross calibrations.

To ease comparison, we report all the light curve measurements in a common set of units. The time axis in both the X-ray and optical plots will be given by the days after the *peak date* of the X-ray outburst. When there is no data for the rising phase, we use the first data point as the peak date. For clarity, the peak calendar date is marked and the truncated Julian date (JD-2440000) is used as the upper abscissa. The intensity axis is given in Crab units or magnitudes in the reported energy or photometric band, while we also plot the energy flux in units of  $\text{ergs s}^{-1} \text{cm}^{-2}$  as the right ordinate.

## 3. LIGHT CURVE MORPHOLOGIES

The most prominent morphological trend we see in the collected light curves is that a large fraction of them have a similar shape: a fast rise followed by an exponential decay (Fig. 1). This is consistent with previous findings (van Paradijs & Verbunt 1984; White, Kaluziński, & Swank 1984). In some cases, the exponential decay lasts for more than 200 days and over 3 orders of magnitude in dynamic range. The *fast-rise-exponential-decay* light curves are also seen in X-ray and  $\gamma$ -ray bursts on much shorter time scales, where they are given the acronym FRED<sup>2</sup>. We adopt this acronym to describe the canonical XN light curves. In cases such as the 1977 outburst of XN 1543–47 (Fig. 1b), the flux decay later becomes erratic – but the *upper envelope* of the light curve maintains an exponential form. We classify these light curves as FREDs also. The best examples of the FREDs are XN 0620–00, XN 1124–683, XN 2000+25, and XN J0422+32, where the first three are recorded in soft X-rays and the last one in hard X-rays. Light curves which have either a fast rise or an exponential decay profile but not both are classified as possible FREDs – examples are shown in Fig. 2.

In addition to the FRED case, we have identified four more general light curve morphologies, *triangular*, *plateau*, *variable decay*, and *multi-peak*, which were not previously recognized. They are illustrated in Figs. 3-7 and listed in Table 5.

The *triangular* profile is one in which the rise time is similar to, or even longer than the decay time

---

<sup>2</sup>This term was coined by Chip Meegan and has now been widely used in the  $\gamma$ -ray literature.

(Fig. 3). The dynamic range of the triangular outbursts is always small so that it is unclear if the rise and decay are exponential or linear.

The *plateau* light curves (Figs. 4-5) are those in which the source stays at the peak ( $\pm 10\%$ ) for an extended period of time ( $> 3$  days). In some cases, the plateau phase is relatively short ( $< 30$  days) and it is followed by a more or less normal exponential decay (Fig. 4). In other cases, the plateau lasts much longer but eventually decays normally (Fig. 5a). In a few extreme cases, however, a very long plateau is terminated by a sudden cutoff (Fig. 5b), thus bypassing the exponential decay phase altogether. No plateaus have been seen in the optical light curves.

The *variable-decay* light curves show an otherwise smooth decay profile broken into several segments, each having a considerably different decay timescale and duration (Fig. 6a, b). In some cases they have a complicated substructure (Fig. 6c). Although the data in Fig. 6a and b are not sufficiently sampled, they clearly show that the decay in the late stages does not follow the same pattern as in earlier stages.

The last morphological type is the *multi-peak* light curve seen only in a few cases (Fig. 7). Different from all other types which have a main outburst, these events undergo several consecutive, *similar* outbursts with later ones sometimes stronger than the first. The three different sources show different timescales in both peak intervals and individual peaks. An important point is that the multi-peak light curves have been seen in both soft and hard X-rays, therefore, they are *not* an exclusive feature of a given energy band.

We have only a very limited collection of optical light curves. Most of them can be classified as FREDs or possible FREDs, as illustrated in Fig. 8.

The light curve morphology can vary not only from source to source but also from outburst to outburst of the same source. For some recurrent sources, different outbursts show similar peak fluxes and durations, e.g., XN 1908+005 (Charles et al. 1980), while for others, different outbursts evolve very differently, e.g., XN 1630–472 (Parmar, Angenili, & White 1995) and XN 1608–52 (Lochner & Roussel-Dupré 1994).

In addition to these major morphological classes, a number of light curves display distinct features, namely the *precursors* and *secondary maxima*, which are superposed on their otherwise canonical profiles. During the rising phase, a small number of outbursts exhibit a weak precursor peak prior to the main peak (e.g., XN 1524–62 and XN 0620–00). In other cases, both the X-ray and optical light curves exhibit one or more *secondary maxima* in the form of a ‘glitch’ (e.g., XN 0620–00 and XN 1124–683), a ‘bump’ (e.g., XN 0620–00), or a series of relatively large amplitude ‘mini-outbursts’ (e.g., XN J0422+32 in the optical). These light curve features will be discussed in more detail in § 5.2.

Finally, we emphasize that: (1) the shapes of the light curves are generally energy dependent with more variability and less uniformity in hard X-rays ( $> 10$  keV) than in soft X-rays, but (2) none of the light curve shapes or features exclusively belong to any given energy band. For example, the *Ginga* light curve of XN 1124–683 in the 1-37 keV band, which is dominated by the soft component ( $< 9$  keV) during the first 150 days, has a proto-typical FRED profile, but the light curve in the 9-37 keV band does not comply with any of the above specified categories (Fig. 9). On the other hand, the 20-100 keV light curve of the 1992 outburst of XN J0422+32 is the best example of a smooth hard X-ray FRED (Fig. 10).

#### 4. Quiescent Emission

Before we discuss the outbursts in detail, let us first examine the properties of quiescent XN emission. Quiescent XNs are usually very faint. Most XNs listed in vP95 have not been detected in quiescence, although the upper limits from previous X-ray instruments are not highly constraining. Recent *ROSAT* and *ASCA* observations of 14 quiescent XNs detected 7 sources and set stringent upper limits on the others. In Table 6, we list for all XNs their quiescent X-ray fluxes or upper limits in col. (5), in units of milli-Crab in the observed energy band. The fluxes are then converted to 0.4-10 keV fluxes in units of  $\text{ergs s}^{-1} \text{cm}^{-2}$ , and listed in col. (6), and to the corresponding luminosities listed in col. (7). In the calculation, we used the spectral information from either the quiescent or the outburst spectrum. When neither was available or not applicable, we assumed a power law of photon index 2.

Table 6 shows that only 9 out of the 24 sources have been detected in quiescence so far. Among them 4 are NSs and 5 are BHCs. We note that the quiescent luminosities of XN 0836–429 and XN 1354–64 seem somewhat high; thus they may have not been seen in their true quiescent state. Table 6 also indicates that the quiescent X-ray luminosity spans several orders of magnitude, particularly for the BHCs. XN 0620–00, for example, has a flux of only  $4.3 \mu\text{Crab}$  in 0.4–1.4 keV (McClintock, Horne, & Remillard 1995), which leads to a record low X-ray luminosity of  $6.2 \times 10^{30} \text{ ergs s}^{-1}$  in 0.4-10 keV. While XN 2000+25 has the lowest flux upper limit of only  $0.36 \mu\text{Crab}$ , its luminosity limit is still higher than that of XN 0620–00, due to its larger distance and absorption column (Verbunt et al. 1994). XN 2023–338, on the other hand, is 4 times brighter and 3 orders of magnitude more luminous than XN 0620 (Wagner et al. 1994). For the NS systems, the spread is much less pronounced. The quiescent luminosities of the 4 NS systems detected so far (XN 0748, XN 1456, XN 1608 and XN 1908) all cluster around  $10^{33} \text{ ergs s}^{-1}$  with a small dispersion of  $\Delta L_q / \langle L_q \rangle = 0.65$ . For the 3 detected BHCs (XN 0620, XN 1655, and XN 2023), the dispersion is 1.61.

The quiescent mass accretion rates listed in col. (8) of Table 6 are derived from  $\dot{M}_q = L_q / \eta c^2$  where we have assumed a radiation efficiency of  $\eta = 0.1$ . These numbers should be taken with caution, since it is possible that many of these systems involve an advection dominated accretion flow (ADAF), which radiates with a very low efficiency (e.g., Narayan, McClintock, & Yi 1996; Narayan, Barret, & McClintock 1997). If in fact  $\eta$  is much smaller, the corresponding  $\dot{M}_q$  will be proportionally higher. We note that much insight into the outburst mechanism and the quiescent state of the system may be gained by comparing the quiescent mass accretion rate derived here with the average mass transfer rate from the secondary star,  $\dot{M}_2$ . The latter has only been inferred for a few sources from the average mass accretion rate required to power the observed outbursts during the period since last outburst (van Paradijs 1996):  $1.3 \times 10^{-11} M_\odot \text{ yr}^{-1}$  for XN 0620,  $1.0 \times 10^{-11} M_\odot \text{ yr}^{-1}$  for XN 1456,  $1.6 \times 10^{-10} M_\odot \text{ yr}^{-1}$  for XN 1908, and  $2.0 \times 10^{-10} M_\odot \text{ yr}^{-1}$  for XN 2023 (see also § 7).

### 5. PROPERTIES OF XN LIGHT CURVES

#### 5.1. Basic Light Curve Properties

While the XN light curves display several different morphologies, most of them can still be characterized by a common set of parameters. An ideal FRED-type X-ray light curve is completely describable in terms of the peak flux  $F_p$  or amplitude  $F_p/F_q$ , the rise timescale  $\tau_r$ , and the decay timescale  $\tau_d$ . This is more or less true for most other types of light curves. Even for the multi-peak light curves, we can use these

parameters for a single peak to represent the entire light curve. Another important quantity is the duration of the outburst which however, except in a few cases, is instrument dependent. In Table 7 we list these basic observational properties of the XN light curves. Col. (2) gives the year and month of the outburst peak. Col. (3) gives the light curve morphology type, as defined in § 3 and Table 5; Col. (4) gives the satellite/instrument and its energy band for which the peak X-ray flux in Col. (5) is reported in Crab units; Col. (6) gives the luminosity in the same energy band; Cols. (7)-(9) give the X-ray rise timescale  $\tau_r$ , decay timescale  $\tau_d$ , and total duration  $T_{\text{obs}}$  respectively. Cols. (10)-(14) give the corresponding optical data, with Col. (11) giving the brightness change (or lower limit) in magnitudes. Col. (15) gives the main references from which the data were obtained. We will discuss each of these quantities separately following the time sequence of an outburst.

### 5.1.1. Rise timescales

A complete empirical picture of how an XN outburst rises from quiescence to the peak has not yet been established. From Figs. 1–5, however, we see that a large portion of most of the *observed* rising phases takes an approximately exponential form, which in some cases holds well for more than 2 orders of magnitude. Moreover, the steepest flux increase seems always to be exponential and it dominates the last decade of flux increase, although the flux increase usually slows down significantly near the peak. In this paper we define the rise timescale  $\tau_r$  to be the e-folding time over the time period which experiences the fastest flux increase. This quantity is readily measurable for most light curves, is instrument independent, and is directly comparable with the commonly used e-folding decay timescale. The results are listed in col. (7) of Table 7. In cases where we have only two data points between the first detection and the peak, we assume an exponential rise between these two points. The corresponding rise timescale will be an upper limit to its true value.

In Table 7 we see that: (1) the rise timescales are generally of the order of a few days but with a large spread,  $\langle \log(\tau_r) \rangle = 0.533 \pm 0.621$  which corresponds to a mean  $\tau_r$  of 3.4 days and the 1- $\sigma$  upper and lower bounds at 14.3 and 0.8 days.<sup>3</sup> Fig. 11 shows that  $\tau_r$  in logarithmic scale is, surprisingly, evenly distributed between 0.6 and 30 days with a narrow peak at the 1–2 day bin (or it is at least a very broad peak if the true values of the two upper limits were smaller by a few bins). Due to limited statistics, we do not know if this indicates two different types of flux increase mechanisms; (2) about 25% of the outbursts have  $\tau_r > 10$  days. This is partly due to the lack of pre-peak coverage (e.g., XN 1354 in 1967 and XN 1630 in 1971) which always makes  $\tau_r$  longer. Several outbursts with long  $\tau_r$ , however, do have adequate rise phase coverage (e.g., XN 1354 in 1987, XN 1915 in 1992, and XN J1655 in 1996), and therefore, are truly slow risers.

The rise timescale so defined characterizes the rate of flux increase but not the *duration* of the rising phase. If a major portion of the flux increase follows a single exponential form, which has been seen in many cases such as XN 1124 and XN 2000, we can define the expected duration of the rising phase to be the rise timescale multiplied by the total number of e-folds from quiescence to peak, i.e.,

$$T_{r,\text{exp}} = \tau_r \ln A_p, \quad (1)$$

---

<sup>3</sup>Due to large dynamical ranges and asymmetric distribution properties, the mean and standard deviation for  $\tau_r$  and most other light curve parameters in the following sections are calculated in logarithmic scale; for convenience, we also report the corresponding mean value and 1- $\sigma$  boundary in their natural units, in the format of *mean (upper bound, lower bound)*.



where  $A_p = L_p/L_q$  is the outburst amplitude which we will discuss later. Therefore, an outburst with  $\tau_r = 3$  days and an amplitude of  $10^3$ , would likely have a rising phase lasting at least about 7 e-folding times, or 3 weeks.

We note that  $T_{r,\text{exp}}$  as defined serves only as a general gauge or a lower limit to the true duration of the rising phase, since the real rising phase may be more complicated than a single exponential form so that a small  $T_{r,\text{exp}}$  does not necessarily imply a short rising phase. The rising history of XN 1524 in 1974 (Kaluziński et al. 1975) consists of two periods with different e-folding times, separated by a precursor peak (Kaluziński et al. 1975). The 2.9-day rise timescale listed in Table 7 is for the second, main period. In this case, the last decade of flux increase took 22 days instead of 6.7 days expected from a single exponential.

Although there has been no complete optical coverage during the rising phase of any XN outburst, there is evidence that the optical light may rise and peak before the X-rays do by at least a few days. For the 1996 outburst of XN J1655–40, Orosz et al. (1997) reported for the first time optical observations fortuitously taken 6 days before the recorded rise of the X-rays, which clearly show that the optical rises *before* the X-rays. In that particular event it is also the case that the soft X-ray rise precedes the hard X-rays (Hynes et al. 1997). However, there is no follow-up data to confirm that the optical actually *peaks* before the X-rays do. For the 1989 outburst of XN 2023, the optical light does peak before the X-rays (Fig. 12), although we do not have a complete optical rise profile due to large variability. There is also weak evidence in the early phase of the 1991 outburst of XN 1124 suggesting that the optical might have peaked 3 days before the X-rays (Della Valle, Jarvis, & West 1991).

### 5.1.2. Peak flux, luminosity and amplitude

At the peak of an outburst, the observed X-ray flux measures the apparent brightness and the luminosity gives the intrinsic energy output. However, the fluxes and luminosities listed in Table 7 have to be converted into common energy bands before meaningful comparisons can be made. Another useful quantity is the outburst amplitude, i.e., the fractional change in the bolometric luminosity from the quiescence to the peak, which reflects the strength of the outburst. Since for most historical XNs, the spectral information that is available is often insufficient for a reliable bolometric correction to be made, we opt to compare the luminosities in a *common* energy band which contains a major portion of the radiated power during both the outburst and quiescence.

We first have to determine the best choice for this common energy band. Historical XN outbursts were recorded by different instruments but they often overlap more or less at the 2-10 keV band (except *Compton*/BATSE, see Table 7). More importantly, a large fraction of the power is radiated in this band for a thermal spectrum of  $kT \sim 1$  keV or a power law spectrum of photon index  $> 2$  or a combination of both. In quiescence, on the other hand, many sources observed by *Rosat* (0.4-2 keV) show a thermal component of  $kT \sim 0.1$  keV. Therefore, a broad band of 0.4-10 keV is likely to encompass much of the total radiated power of XNs in both outburst and quiescence. Converting the observed fluxes obtained by most X-ray instruments to this common energy band does not require large extrapolation and thus should not introduce large uncertainties.

Using the published spectral parameters and peak fluxes (Table 7) we calculated, in the 0.4-10 keV band for each outburst, the calibrated outburst peak X-ray flux  $F_p$  in units of  $\text{ergs s}^{-1} \text{cm}^{-2}$ , peak luminosity  $L_p$  in units of both  $\text{ergs s}^{-1}$ . We also computed the Eddington luminosity,  $L_{\text{Edd}} \sim 1.3 \times 10^{38} \text{ ergs s}^{-1} (M/M_\odot)$ , assuming solar composition, and peak amplitude  $A_p = L_p/L_q$ . The results are listed in Table 8.

It is seen that the peak flux,  $F_p$ , spans 4 orders of magnitude ranging from  $1.22 \times 10^{-10}$  (XN 1630–472 in 1979 March) to  $1.35 \times 10^{-6}$  ergs s $^{-1}$  cm $^{-2}$  (XN 1456–32 in 1969 July), with  $\langle \log(F_p) \rangle = -7.84 \pm 0.82$  with the corresponding the mean and 1- $\sigma$  boundary for  $F_p$  at  $1.4 (9.5, 0.2) \times 10^{-8}$  ergs s $^{-1}$  cm $^{-2}$ . The peak luminosity, on the other hand, varies from  $8.6 \times 10^{35}$  ergs s $^{-1}$  (XN 0748, 1985 February) to  $8.63 \times 10^{39}$  ergs s $^{-1}$  (XN 1742, 1975 February), and  $\langle \log(L_p) \rangle = 37.72 \pm 0.79$  or  $0.52 (2.22, 0.08) \times 10^{38}$  ergs s $^{-1}$ .

In deriving  $L_p/L_{\text{Edd}}$  we have assumed a mass of  $1.4M_\odot$  for a NS and  $10M_\odot$  for a BH for sources whose compact object mass is not available. We see that  $L_p/L_{\text{Edd}}$  ranges from 0.0031 (XN 0042+32, 1970 February) to 6.6 (XN 1742–289, 1975 February). The mean is  $\langle \log(L_p/L_{\text{Edd}}) \rangle = -1.00 \pm 0.68$  or equivalently the mean  $L_p/L_{\text{Edd}}$  and its 1- $\sigma$  boundary at 0.10 (0.48, 0.02). This result deviates from the general belief that the peak luminosity of XN outbursts is always near the Eddington limit. Changing the unknown BH masses from  $10M_\odot$  to  $5M_\odot$  only increases this value by a factor of  $< 2$ . When we count only the most luminous outburst from each source, the average luminosity increases to  $0.13 (0.97, 0.02)L_{\text{Edd}}$ . In Fig. 13 we plot the distribution of the peak luminosity in Eddington units. It is roughly a Gaussian centered at  $0.2L_{\text{Edd}}$  with a FWHM of 0.82 in logarithmic scale, if we disregard the large excess at  $< 0.03$ . These values may have been biased by the uncertainties in the distances, masses, and spectral shapes, especially in the case of XN 0042+32, XN 0836–429, and XN 1918+146. The cases with  $L_p/L_{\text{Edd}} > 1$  are probably also biased by these uncertainties.

Next, we examine the outburst amplitude  $L_p/L_q$ , listed in col. (5) of Table 8. For sources only having upper limits for their quiescent fluxes, we calculate the lower limits of their outburst amplitudes. We see that the peak amplitude varies from only a factor of less than 2 for XN 0836–429 in 1990 May to an astonishing  $2 \times 10^7$  for XN 0620–00 in 1975 August. The average amplitude is  $(7.17 \pm 0.78) \times 10^3$ . If we exclude the lower limits, the average increases by a factor of  $\sim 2$  to  $(1.54 \pm 0.08) \times 10^4$ ; if we take only the highest amplitude from each of the 9 positively detected sources, the average amplitude jumps by another factor of  $\sim 2$  to  $(3.73 \pm 0.16) \times 10^4$ . Fig. 14a shows that the amplitude distribution in logarithmic scale has a broad peak at  $\sim 10^4$ . Future detections of quiescent fluxes will make the distribution move to the right.

One may ask if there is a difference in the amplitude distribution between the BHs and NSs. Fig. 14b-c shows that the NS events have a narrow distribution around  $\sim 10^4$ , dominated by the recurrent events of XN 1608–522 and XN 1908+005. If we take only one outburst from each source, however, the amplitude distribution of NS events is similar to that of the BHs, i.e., a broad hump between 10 and  $10^7$ . We note that most BH events have only a lower limit on their amplitude and the true distribution may be different from the one shown here. For the same reason, the lack of BHCs events in the bins of  $10^4$  and  $3 \times 10^4$  seems to be accidental.

### 5.1.3. Decay timescales

For most XN light curves, we can define the decay timescale  $\tau_d$  as simply the e-folding time computed over a time period long enough to smooth out small scale variations. Generally speaking,  $\tau_d$  is a well determined parameter, because the overall shape of most light curves, or the upper envelope of variable light curves, is approximately exponential in both the X-rays and optical. When the observed flux range is small, we may not be able determine with confidence if the decay is exponential, linear, or a power law. In these cases, we assume it is exponential. For plateau or variable decay profiles, we calculate  $\tau_d$  for the dominant phase of the decay. For example, for a short plateau profile we use the decay timescale of the

normal decay phase which is usually longer than the plateau phase. For a long plateau we list the quantity  $\tau_d$  which characterizes the decay timescale *during* the plateau phase.

A prominent trend found in historical XN light curves is a universal decay timescale of approximately 30 days (White, Kaluziński, & Swank 1984). This feature still holds in our enlarged sample,  $\langle \log(\tau_d) \rangle = 1.24 \pm 0.36$  or equivalently 17.4 (39.8, 7.8) days, after excluding the plateau events. Although the spread is still large, Fig. 15 shows that the distribution of  $\tau_d$  is quite different from that of  $\tau_r$ . Here, we see an approximately Gaussian profile in the logarithmic scale, which peaks at  $\sim 24$  days, and with a FWHM of 0.65 in  $\log \tau_d$ . The large spread is mainly caused by significant residues at both short and long timescales.

Considering the large intrinsic differences among these systems, the observed universality of the exponential decay and its time constant are remarkable and likely to be the results of some fundamental physical processes involved. From Table 7 we also find that for recurrent sources, the universality holds for multiple events of *similar intensity* (e.g., XN 1908+005 in 1975-1978), but not for multiple events of *different intensity* (e.g., XN 1456-32, XN 1608-522, XN 1630-472). Looking for a possible dependence of the decay timescale on some other physical quantity, we notice that, as shown in Fig. 16,  $\tau_d$  of high luminosity outbursts (excluding the plateau events) seems to be confined to a much narrower range than that of the low luminosity outbursts.

The limited statistical information available on optical decay timescales in our sample allows only for crude conclusions to be drawn. First, the flux decay is generally a factor of 2.2 slower in the optical than in X-rays. From Table 7 we derive an average decay time of 67.6 days in the optical and 34.9 days in X-rays (excluding the long plateaus). For individual outbursts, this ratio is 1.5 for XN 1908+005 in 1978 and 4.8 for XN J0422+32.

#### 5.1.4. Duration and total energy

The observed duration of the outbursts, listed in Table 7 for the X-rays ( $T_{\text{obs}}$ ) and optical ( $T_{\text{obs,o}}$ ), is the total elapsed time in days between the first and the last detections of the source. This is clearly dependent on the instrumentation and on the conditions under which the observations were made. Similarly to both the rise and decay timescales, the observed duration has a large spread in time ranging from  $\sim 10$  days to  $> 100$  days with a mean value of  $\langle \log(T_{\text{obs}}) \rangle = 2.05 \pm 0.42$  which corresponds to the mean and 1- $\sigma$  boundary of 112 (294, 43) days. For the small number of observed  $T_{\text{obs,o}}$ , these values are  $2.02 \pm 0.50$  and 104 (327, 33) days. We have searched for, but found no correlation between the duration and either the peak flux or the amplitude.

Since  $T_{\text{obs}}$  is highly instrument dependent, we define an expected duration to be more reflective of the intrinsic event. First, similarly to the rise phase duration  $T_{r,\text{exp}}$ , we define the expected duration for the decay phase to be the number of days required for the outburst to decay from the peak to quiescence, i.e.,

$$T_{d,\text{exp}} = \tau_d \ln A_p. \quad (2)$$

Then, the expected duration of the entire outburst is defined as

$$T_{\text{exp}} = T_{r,\text{exp}} + T_{d,\text{exp}} = (\tau_d + \tau_r) \ln A_p. \quad (3)$$

This quantity is still instrument dependent in the sense that some of the amplitudes are only upper limits. Using the observed rise and decay timescales (Table 7) and the calibrated outburst amplitudes (Table 8),

we calculate  $T_{r,\text{exp}}$ ,  $T_{d,\text{exp}}$  and  $T_{\text{exp}}$ , and the results are listed in Table 9. We see that  $T_{\text{exp}}$  is usually a factor of 2 or more longer than  $T_{\text{obs}}$ .

A measure of the energetics of an XN outburst is the total radiated energy, i.e., the time-integrated X-ray luminosity over the entire outburst. For outbursts which follow an exponential profile during both the rising and decay phase, the expected total energy of the outburst can be calculated as

$$\begin{aligned} E_{\text{exp}} &= L_{\text{p}}[\tau_{\text{r}}(1 - e^{-T_{r,\text{exp}}/\tau_{\text{r}}}) + \tau_{\text{d}}(1 - e^{-T_{d,\text{exp}}/\tau_{\text{d}}})] \\ &= L_{\text{p}}(\tau_{\text{r}} + \tau_{\text{d}})(1 - A_{\text{p}}^{-1}). \end{aligned} \quad (4)$$

For  $A_{\text{p}} \gg 1$ , we have  $E_{\text{exp}} \sim L_{\text{p}}(\tau_{\text{r}} + \tau_{\text{d}})$ . This formula does not include the irregularities in the light curves, nor does it take into account a possible spectral evolution during the outburst as seen, for example, in the 1991 outburst of XN 1124–683 (Ebisawa et al. 1994). From the observed light curves, however, we know that the irregularities in general will not affect the derived total energy by more than a factor of 2, and substantial spectral evolution occurs only when the X-ray flux has decayed significantly. Therefore, the total energy estimated here is in general accurate, to about a factor of 2-3. In Table 9 we list the derived total energy for sources with sufficient data. It is seen that this quantity covers 4 orders of magnitude in dynamic range with  $\langle \log(E_{\text{exp}}) \rangle = 44.47 \pm 1.01$  which corresponds to the mean and (upper, lower)  $1-\sigma$  boundary for  $E_{\text{exp}}$  of  $2.92 (29.8, 0.3) \times 10^{44}$  ergs. This corresponds to (on average) a total amount of mass  $\Delta M = E_{\text{exp}}/\eta c^2$  of  $1.64 (16.7, 0.16) \times 10^{-9} M_{\odot}$  being accreted on to the compact object during an XN outburst, where we assume a radiation efficiency  $\eta = 10\%$ . The distribution of  $E_{\text{exp}}$  in Fig. 17 shows a broad hump centered at around  $10^{44}$  ergs.

## 5.2. Additional Light Curve Features

### 5.2.1. Precursors

The rising phase of most XN outbursts is characterized by a fast, monotonic flux increase. In a few cases, however, it exhibits a *precursor* peak prior to the main peak. The best example is the 1974 outburst of XN 1524–62 recorded by *Ariel 5* (Fig. 18a). Its 3–6 keV flux reached a local maximum of  $\sim 80\%$  of the main peak about two weeks before the main peak. The rising to the precursor peak was slightly slower than that to the main peak. After the precursor, the 3–6 keV flux declined by a factor of 2 followed by a rapid rise to the main peak. A less prominent precursor was seen in the 1975 outburst of XN 0620–00, which crested at  $\sim 10\%$  of the main peak about a week earlier, although this is evident only in a linear light curve plot (Fig. 18b). There is also weak evidence for a precursor in the outbursts of XN 1608–522 in 1970, XN 1730–220, XN 1915+105, and XN 1908+005 in 1975. While there are not enough cases for a statistical treatment, the lack of other clear examples probably indicates that precursors are not a common phenomenon.

The precursors we discussed above may be of a different physical origin from the often more structured light curves seen in high energies, as illustrated by the case of XN 1124–683. The *Ginga* 1–37 keV light curve shows only a monotonic rise, but in 9–37 keV it clearly exhibits two peaks (Fig. 19b): one 7 days before the main peak (in 1–37 keV), with  $80\%$  of  $F_{\text{p}}$  and another 6 days after the main peak with  $60\%$  of  $F_{\text{p}}$ . The 6–15 keV light curve from *Granat*/WATCH, on the other hand, has 3 peaks at –6 days ( $\sim 20\%$  of  $F_{\text{p}}$ ), –3 days ( $\sim 25\%$  of  $F_{\text{p}}$ ), and 7 days ( $\sim 12\%$  of  $F_{\text{p}}$ ) (Fig. 19a). Finally, the WATCH 15–150 keV light

curve also shows 3 concurrent peaks with different flux ratios (Fig. 19c). Such a complexity suggests that (1) an XN outburst may peak at different times in different energies, (2) the hard X-rays usually rise and peak earlier than the soft X-rays (while as noted in (§ 5.1.1) the optical may peak before both the hard and soft X-rays), and (3) the precursor phenomenon is a rare feature in the low energy light curves, while the multi-peak behavior is more common in high energy light curves.

### 5.2.2. Plateaus

We have discussed the plateau events and classified them as one of the major morphologies of the XN light curves, but this phenomenon warrants some further discussion. In Table 10 we list the decay timescale during the plateau phase ( $\tau_{\text{plt}}$ ), the duration of the plateaus ( $T_{\text{plt}}$ ), and the decay timescale during the subsequent decay phase following the plateau ( $\tau_{\text{tail}}$ ). For the plateau events XN 1705–25 in 1977, XN 1716–249 in 1993, and XN 1915+105 in 1992, the plateau decay constant  $\tau_{\text{plt}}$  is the same as  $\tau_{\text{d}}$  listed in Table 7. The events in BH systems are listed separately from those in the NS systems. Generally speaking, a large spread in both the decay timescale and duration, and in the subsequent decay behavior is evident for both BHs and NSs. After the plateau (long or short) phase, the sources usually take on a normal exponential decay, but occasionally undergo a sharp cutoff. This can happen in both BHs and NSs.

One thing is striking in Table 10 – on average, all measures of the plateau durations in BHs are longer than those in NSs by a factor of 2 or more. For the BHs, even after excluding the extreme case of XN 1915+105, we get  $\langle \tau_{\text{plt}} \rangle = 338$  days,  $\langle T_{\text{plt}} \rangle = 45$  days, and  $\langle \tau_{\text{tail}} \rangle = 34$  days, respectively, which are still substantially longer than those for the NSs. Individually, XN 1915+105 in 1992 (Fig. 5c) holds the record in both the decay timescale ( $\sim 2400$  days) and plateau duration ( $\sim 300$  days), which makes it the most energetic ( $E_{\text{exp}} \sim 2.8 \times 10^{46}$  ergs) XN event ever.

With the exception of XN 1915+105, the longest plateau occurred in XN 1716–249 (Fig. 5b), also a BHC. Both XN 1716 and XN 1915 underwent another, though much shorter outburst of similar peak flux about 200 days after the end of the plateau phase. In other words, these two sources seem to be turning back on again very soon after their large, initial outbursts. We do not know if these later events are entirely separate outbursts or “mini-outbursts” associated with the decay phase of a previous outburst. It is nevertheless somewhat puzzling that these sources have managed to accumulate enough material to trigger the subsequent outbursts. We note that except for these light curve similarities, the two sources are quite different: the peak X-ray spectrum of XN 1716–249 has no soft component whereas XN 1915+105 has; XN 1915 is an extremely slow riser whereas XN 1716 is fast; XN 1915 is a superluminal jet source while XN 1716 is apparently not, although it has weak radio emission and Hjellming et al. (1996) have suggested that its X-ray-to-radio may be a low intensity analog of the superluminal sources XN J1655 and XN 1905.

### 5.2.3. Secondary maxima

Even in the canonical FRED light curves, the exponential decay may not always be strictly monotonic. Instead, it is often interrupted by flux increases by a factor of two or more, followed by resumption of the normal decay; thus displaying *secondary maxima* (Chen, Livio, & Gehrels 1993).

There are three morphological types of secondary maxima observed to date: *glitches*, *bumps*, and

*mini-outbursts*.<sup>4</sup> A glitch is an upward inflection superposed on a smooth exponential decay, i.e., after the glitch the decay follows roughly the same path as before, but is offset upwards by a factor of  $\sim 2$  or more. Glitches are seen in the X-ray light curves of XN J0422+32 (Fig. 10), XN 0620–00 (Fig. 20), XN 1124–683 (Fig. 9), XN 1543–47 (Fig 1b), and XN 2000+25 (Fig. 1a). We note that a glitch is always the *first* secondary maximum to appear in a light curve within 100 days after the peak, irrespective of how many additional features may occur subsequently. Glitches have also appeared in the optical light curve of XN 0620–00 (Fig. 20) and possibly of XN 1456–32 (Fig. 8a), and in the UV light curves of XN J0422+32 and XN 1124–683 (Fig. 21), at about the same time as in the X-rays.

On the other hand, both “bumps” and “mini-outbursts” are small-amplitude (relative to the primary peak) events superposed on a normal decay profile, except that in some cases the mini-outbursts appear to be more like outbursts by themselves, i.e., when the source is closer to quiescence. Bumps have been seen both in X-rays from XN 0620 (Fig. 20) and XN 1124 (Fig. 9) and in the optical from XN 0620 (Fig. 20), while mini-outbursts have been seen only in the optical from XN J0422 (Fig. 10) and XN 1009 (Fig. 22). XN J0422+32 provided the most dramatic example of mini-outbursts approximately one year after its initial outburst (Shrader et al. 1997). Its R-band light curve is clearly divided into two phases separated by a precipitous decrease of more than 4 magnitudes  $\sim 220$  days after the peak. It is remarkable that in both phases the baseline decay rates are almost the same. Even more intriguing is the fact that the mini-outbursts temporarily brought the flux back to a level consistent with an extrapolation of the first-phase decay curve! Therefore, the occurrence of the mini-outbursts may be causally related to the earlier flux “free-fall”.

Like other light curve properties, the secondary maxima are energy dependent. The glitch in the 1991 outburst of XN 1124–683 about 70 days after the peak appears clearly in *Ginga*’s soft (1-5 keV) band, is less apparent in the medium (5-9 keV) band, and is not seen at all in the high energy ( $> 9$  keV) band (Tanaka, Makino, & Dotani 1991; Ebisawa et al. 1994). Therefore, it is a soft X-ray feature, similar to the one seen in XN 0620–00 which has an accompanying optical feature. On the other hand, the prominent glitch which appeared in the 20–100 keV light curve of XN J0042+32 has no apparent counterpart in the optical (Fig. 10), suggesting that the optical/UV glitches are decoupled from the hard X-ray glitches. Furthermore, a glitch appeared in the UV light curves of both XN 1124–683 and XN J0422+32, at about 70 days and 45 days after the peak, respectively (Shrader et al. 1994). It is striking that in both cases, the glitch is more prominent in the 1300Å than in the 2600Å light curve, thus strongly hinting at a common origin for the X-ray and UV behavior (Shrader et al. 1994). We should also point out that while the UV glitch in XN 1124–683 coincides with the one in soft X-rays, in XN J0422+32 there is no counterpart either in the optical, although the data are noise limited, or in hard X-rays by BATSE (20–100 keV), where there is at most a marginal deflection.

#### 5.2.4. Multi-peak light curves

The multi-peak light curve occurs only in a few cases, and its puzzling nature deserves some brief discussion in this section. First, XN J1655–40 is a truly unusual source, for its multi-peak light curve (Fig. 7), but more importantly for its superluminal jets. Like the two long plateau sources XN 1716-249 and XN 1915+105 (the only other Galactic superluminal jet source), XN 1655–40 has not been detected in the

---

<sup>4</sup>Following the terminology adopted at the 1996 Aspen Winter Workshop on Black Hole X-Ray Transients.

last two decades and it became active only recently. In its 1994 outburst, it underwent several consecutive outburst peaks with an interval of  $\sim 120$  days (Harmon et al. 1995). Unlike XN 1915 or XN 1716, however, its first peak is not the largest one in either flux or duration. Some of the peaks are followed by radio flares but some are not (Hjellming & Rupen 1995). The light curves of the individual peaks are not FREDs but more or less triangular with roughly equal rise and decay timescales. A similar multi-peak light curve does not show in the 1996 outburst of XN 1655, which is nevertheless characterized by an extremely slow and erratic rise and decay.

The multi-peak light curve of XN 0042+32 in a weak (0.03 Crab) outburst in 1977 (Watson & Ricketts 1978), resembles the 1994 outburst of XN J1655–40 (Fig. 7). Similarly, the light curves for individual peaks are approximately triangular and the first peak is not the strongest. The only apparent difference from XN 1655 is that the quasi-periodical peak interval, in this case, is 11.6 days instead of 120 days. It is important to note, however, that XN 0042 was detected in the 3–6 keV band, so that a multi-peak light curve behavior occurs in both hard and soft X-rays.

## 6. DISTRIBUTION OF X-RAY NOVA SYSTEMS

### 6.1. Frequency of XN Outbursts

Now we address the question: what is the overall rate of XN events in the Galaxy? This is a nontrivial question because it depends on the sky coverage, lifetime, limiting sensitivity and the energy band of X-ray instruments launched at different times over the last 30 years. In our attempt to quantify the sky coverage over this period of time, as a fraction of the full sky over which an XN would be detected, a number of simplifications were involved. First, we did not distinguish among coverages in different energy bandpasses. *Compton*/BATSE for example, even though with no sensitivity below 20 keV, has discovered three new XNs and detected recurrent emission from several others during its initial 4 years of operation, while the peak XN emission is often thought to be in the 2–10 keV band. Second, we have not attempted to calibrate the sky coverage of various satellites according to their sensitivities, which often differ considerably for the multiple experiments and/or multiple modes a satellite may have operated on (e.g., HEAO 1 scanned during the initial mission phase and was subsequently pointed). The limiting sensitivities of the different instruments varied widely, but most were able to detect transient sources to a level of  $\sim 0.1$  Crab. However, it does not simply suffice for the peak intensity to reach (or slightly exceed) this threshold for an event to be registered as an XN outburst. Sufficient data are needed to allow a characterization of the transient, thus a more realistic threshold is  $\sim 0.3 - 0.5$  Crab. It is also somewhat subjective to attempt to identify what truly constitutes the detection probability for a given source and instrument configuration and solid angle coverage. Short-lived and relatively faint events could easily go undetected by a state-of-the-art ASM like XTE if they happened to occur within the nominal 10% of the sky included in the solar or SAA zones of avoidance.

Keeping all of these caveats in mind, we computed an approximate XN rate by averaging over the nominal 30-year coverage baseline, and including *all types* of events, BHC, NS, and sources of unknown nature. Not included are the 11 “Possible XNs” in Table 3, which would have clearly shifted the estimated rates upwards. The upper panel of Fig. 23 is a histogram based on all the qualified 50 events. The estimated sky-coverage factor is illustrated in the lower panel, this was calculated by considering the instrumental capabilities and mission lifetimes of 14 different satellites, as well as sounding rocket programs of the late 1960’s (Table 11). In some cases, it was necessary to apply some subjectivity; for example, we assigned

sky-coverage factors of  $\sim 10\%$  to scanning experiments such as *HEAO 1* and *UHURU*. All-sky monitors were assigned values of 80%–90%. On the basis of all of the above, we estimate a rate of  $\sim 2.6$  XN outbursts per year. The corresponding nominal rates for the NS and BH subgroups are  $\sim 1.1$  and  $\sim 1.5$  respectively.

## 6.2. Recurrence Times and Properties of Recurrent Sources

Many XNs are known to have undergone more than one outburst. XN 0620–00 (XN Mon 1975) reached a similar optical brightness during an outburst in 1917 (Eachus et al. 1976). XN 2023+338 (V404 Cyg) also erupted in 1938 (Wachmann 1948), 1956 and possibly 1979 (Richter 1989). The BHC XN 1630–472 has undergone quasi-periodic outbursts every  $\sim 600$  days since 1969 (Parmar, Angenili, & White 1995). Thus, the reported recurrence time in different systems varies from about 1 to 60 years.

In Table 7, more than 50% (13 of the 24) of the XN sources have more than one outburst and 6 of them have at least 3 outbursts. If we take all the recurrent events and ignore the possibility of missing events between some of the recorded outbursts, we see that the maximum recurrence time is 57.8 years (XN 0620) and the minimum is 0.25 years (XN 1608–522). The mean recurrence time in logarithmic scale is  $0.41 \pm 0.54$  which corresponds to an mean and  $1-\sigma$  (upper, lower) boundary for  $T_{\text{rec}}$  of 2.6 (8.9, 0.7) years. Fig. 24 shows the distribution of the recurrence times. It has a sharp peak around 1 year and a broad base. The true distribution is likely to be affected by two factors. On one hand there must exist some missed outbursts between some of the recorded events, which will increase the count of short recurrence times. On the other hand, some of the sources which currently have only one recorded outburst (and therefore are not included in Fig. 24) may go into outburst in the future, thus increasing the count of long recurrence times.

For recurrent XNs, the peak flux, duration, and light curve morphology often differ from outburst to outburst. The question is then: are there any systematic differences between the strong and weak outbursts? For example, in § 5.1.3 we have seen that the decay timescale  $\tau_d$  of the strong outbursts has, on average, a much narrower distribution (around 30 days) than that of the weak outbursts. The question is, does this property hold also for multiple outbursts from the same source? An examination of Table 7 for XN 1543–47, XN 1630–472 and XN 1908+005, reveals that this is not the case. For the two recurrent XNs in the Centaurus region, XN 1354–64 (a BHC) and XN 1456–32 (a NS), Fig. 25 shows an opposite trend. The strong outburst of 24 Crab from Cen X-2 in 1967 (although its identification with XN 1354–64 is only tentative) decayed twice as fast as the weak outburst in 1987 which was about 100 times fainter. The strong outburst of  $\sim 30$  Crab of XN 1456–32 in 1969, on the other hand, decayed 5 times more slowly than the weak outburst 10 years later which was 7 times fainter. Thus, it appears that there is no correlation between the outburst magnitude, duration and decay timescale. We also do not find any clear correlation between the recurrence time and the outburst luminosity.

## 6.3. Spatial Distribution

In Fig. 26 we have plotted the positions of 24 XNs on a Galactic-Aitoff grid. The symbol sizes have been scaled in approximate proportion to the peak intensities of the events. For multiple outbursts from a single source, we have chosen the brightest outburst for representation in this figure. The different symbols correspond to BH, NS, and unknown systems as detailed in the figure caption. Clearly there is a general



concentration of sources along the Galactic plane, with an additional enhancement associated with the bulge. Considering only the probable neutron star systems, a more irregular distribution is seen with several sources well out of the plane, but any conclusions are limited by the small-number statistics. The BH systems are roughly uniformly distributed along the plane, including several in the general anti-center direction. The tendency for BHC systems to be less concentrated towards the Galactic bulge, unlike the broader class of LMXBs which exhibit a distinct concentration in the bulge region has been noted by White (1994) (see also White & van Paradijs 1996), who suggests that this may be indicative of a tendency for BHC systems to be associated with a Population I distribution. One must be cautious in accepting this interpretation however, since a large fraction of the sources cannot be classified, and a number of the ones which are assumed to be BHCs are at best tentatively classified.

The Galactic disk-bulge distribution of XNs can also be inferred from the  $\log(N) - \log(S)$  relationship of the XN outburst peak fluxes, shown as a histogram in Fig. 27. We have treated recurrent outbursts from the same sources as individual events in this analysis. The dashed line shows a source distribution extending beyond the local range into a disk of infinite size, so that it turns into a power law of  $S^{-1}$  at flux thresholds below  $\sim 30$  Crab. Intuitively, one might expect the actual distribution of XN sources to fit such a distribution, but it is clearly too steep when compared to the observations. We considered the case in which the XN sources are distributed on the Galactic plane (12 kpc in radius), and the observer is located at 8.5 kpc from the Galactic center; this is represented by the dash-dotted line in Fig. 27.

We can attempt to calculate  $\log(N) - \log(S)$  numerically by making some basic assumptions about the luminosity and spatial distributions. From Table 8, we find that the range of X-ray luminosities among events with distance estimates is  $36.0 < \log L_{x,p} < 39.3$ , with a mean value of 37.5. The distribution is approximately symmetric, rather than exhibiting an excess towards the low-luminosity end. We attribute this lack of asymmetry to detection inefficiency rather than to a real physical effect, nonetheless we have approximated the distribution in luminosity as a Gaussian. The spatial distribution of all XNs exhibits an excess in the Galactic bulge region as noted above, although the BHC subsample may be uniformly distributed over the disk. We have modeled this spatial distribution as a constant surface density over the disk plus a  $r^{-3}$  power-law component to represent the apparent excess associated with the bulge. We then performed a numerical integration over these luminosity and space distributions, using again a geometry with the origin offset from the disk center by 8.5 kpc. We derive a  $\log N - \log S$  curve which we can then scale, i.e., vary the mean surface density as a free parameter, to approximately fit the observed  $\log(N) - \log(S)$  distribution at the bright end, where it is presumably reasonably well constrained by observations. The resulting distribution begins to flatten at  $10^{-2}$  Crab, and is flat by  $10^{-3}$  Crab.

By constraining our model to overlay the bright portion of the observed  $\log N - \log S$  distribution and then extrapolating to a flux threshold of  $\sim 10^{-2}$  where it becomes flat, we can estimate the total number of XNs in the galaxy. In this manner we derived a mean surface density of about  $0.25 \text{ kpc}^{-2}$  from which we estimate that there are a few hundred XNs in the galaxy. This estimate is a lower limit in the sense that the true mean recurrence time scale may be much larger than what we infer from the observed subsample as discussed previously. This situation may not be improved upon observationally for decades, although theory of binary star formation and evolution holds promise for the nearer term.

## 7. FROM THE LIGHT CURVES TO THE PHYSICS OF OUTBURSTS

In this section, we discuss briefly some of the theoretical implications of the properties of XN light curves we have found so far. In § 3, we saw that many XN light curves are FREDs or possible FREDs, and most other light curve morphologies are of this basic profile but distorted or stretched in a variety of ways. The question is, therefore, is there a common underlying outburst mechanism which is responsible for at least the majority of the outbursts? And, if so, what constraints do the statistical properties and light curve features discussed in § 5 place on such a model? Finally, if discrepancies exist, where should we look for possible solutions?

There were originally two basic outburst mechanisms which have been suggested. One is the mass transfer instability (MTI) model which attributes the outbursts to a temporary increase in the mass transfer rate from the companion as a result of the continuous X-ray heating of the companion’s surface in quiescence (e.g., Hameury, King, & Lasota 1986, 1990). The other is the disk thermal instability model (DTI) which is based on the existence of two thermal states at a given disk surface density (due to an opacity jump around the hydrogen ionization temperature, e.g., Cannizzo, Ghosh, & Wheeler 1982, Faulkner, Lin, & Papaloizou 1983, Meyer & Meyer-Hofmeister 1984, Huang & Wheeler 1989, Mineshige & Wheeler 1989). More recently it has been pointed out, however, that the MTI model has some severe shortcomings which make it inapplicable to the XN outbursts (e.g., Gontikakis & Hameury 1993, Mineshige, Yamasaki, & Ishizaka 1993). The DTI model (also called the limit cycle model), on the other hand, has been very successful in explaining dwarf nova outbursts (e.g., Cannizzo 1993 and references therein). Recently, Cannizzo, Chen, & Livio (1995, hereafter CCL95) embarked on a series of calculations that enabled to clarify several important properties of limit cycles experienced by disks around BHs. We will thus focus only on the DTI model in our following discussions of each of the observed properties. A related model for the accretion flow in BH systems that has attracted much attention recently is the advection dominated accretion flow (ADAF) model, which appears to be able to successfully explain the quiescent XN spectra and luminosities (e.g., Abramowicz et al. 1995, Narayan, McClintock, & Yi 1996). ADAF models can be incorporated into DTI models for the outburst, as we discuss below.

*Universal exponential decay and its timescale.* An important result of CCL95 is that the DTI model cannot produce exponential decays if the viscosity parameter  $\alpha$  is taken either as a step function between the two stable branches (Huang & Wheeler 1989, Mineshige & Wheeler 1989) or as a function of radius of the form  $r^\epsilon$  (Cannizzo 1993). Robust exponential decays can be reproduced *only* if  $\alpha$  is a function of the local aspect ratio  $h/r$ , of the form  $\alpha = \alpha_0(h/r)^n$  with  $n = 1.5$ . Here  $h$  is the disk scale height at a given annulus of radius  $r$ , and  $\alpha_0$  is a constant. This result is the direct consequence of a more fundamental finding that the width of the transition front in the disk, which transforms the hot state into the cold state and vice versa, is the geometrical mean of  $h$  and  $r$  (CCL95; Vishniac & Wheeler 1996). Therefore, the universality of exponential decay is indeed the result of some fundamental physical processes in the disk. CCL95 have further shown that the decay timescale is proportional to  $M/\alpha_0$  where  $M$  is the mass of the accreting object. This is interesting because under the assumption that  $\alpha_0$  is more or less universal (e.g., if it is determined by a MHD dynamo in the disk), then this seems to be able to explain why the dwarf novae usually have a decay constant of only about 3 days while the BHXNs have a decay constant of  $\sim 30$  days. It is quite clear, however, that this relation is not precise, since the NSXNs have similar decay timescales as the BHXNs even though the mass of NSs is typically smaller than that of BHs by a factor of a few.

*Fast rise.* In the disk instability model, an outburst can be triggered either “outside-in” or “inside-out”, depending on the history of the last outburst and the mass accretion rate through the disk in quiescence.

Cannizzo (1996) found that the fast rises can be obtained only if the outbursts are triggered at radii larger than about  $10^{10}$  cm from the BH (see also Cannizzo, Wheeler, & Polidan 1986). On the other hand, the outbursts are always triggered near the inner edge of the disk ( $\sim 10^7$  cm for standard disks in XN systems) if the mass transfer rate to *the inner edge* is greater than about  $10^{-19} M_{\odot} \text{ yr}^{-1}$  (CCL95; see also Lasota, Narayan, & Yi 1996). This problem may be circumvented if we employ the ADAF model for the quiescent state of the system. In this model, the inner part of the accretion flow (of dimensions of the order of  $10^4$  gravitational radii) is nearly spherical and optically thin, and it joins at a transition radius,  $r_{\text{tr}}$ , to an outer standard accretion disk (e.g., Narayan et al. 1996, 1997). Under these conditions, even outbursts that are triggered at the inner edge of the standard disk (at  $r_{\text{tr}} \sim 10^{10}$  cm) are in fact started at large radii, thus might be able to produce a fast rise in X-rays.

A relative weakness of the ADAF model is the lack of a fully convincing physical mechanism to remove the inner part of the disk at the end of the outbursts and/or during quiescence. Therefore, the exact location of the transition radius (the inner edge of the quiescent disk) is not determined by the theory (although it can be constrained by the requirement of stability). However, this may reflect the real situation in the sense that the uncertainty in the location of the inner edge of the quiescent disk may naturally lead to a broad distribution of the rise timescales in outbursts, similar to what we see in Fig. 11. An important corollary is that the existence of outbursts with a very slow rise may imply that there is no ADAF in operation in the quiescent state of these sources. We also note that because of the requirement for the standard disk to first fill in (by diffusion) the central parts occupied by the ADAF at quiescence, one would expect naturally a delay in the rise of the X-ray flux, relatively to the rise in the optical such as the one observed in XN 1655–40 (Orosz et al. 1997). Similar models, including a hole at the center of the disk to explain the UV delay, have been proposed for dwarf novae (e.g., Livio & Pringle 1992).

*The diversity of XN light curve morphologies.* It is presently unclear if the variety of light curves observed in XN outbursts, such as, plateaus and triangular profiles, can all be explained by a disk instability model. Nevertheless, it should be noted that a wide range of outburst behaviors in dwarf novae have been successfully modeled by a disk instability (Cannizzo 1993), and that the light curves that were obtained do include both plateau and triangular outbursts.

Naively, one might think that multi-peak outbursts may be due to a different physical mechanism than that responsible for the “normal” XN outbursts. However, a strong piece of evidence against this notion may be the fact that these and most other XNs included in our study all have spent a long time in quiescence before their first eruption, which suggests that the physical mechanism which keeps these sources dormant may be universal. It is probably due to the external conditions, such as the binary parameters, the nature of the secondary mass-donor star, and especially its response to the X-ray irradiation during outburst, which are responsible for the diverse nature of the XN light curve morphologies and features.

*Secondary maxima.* There has been so far no single satisfactory mechanism to explain the observed variety of secondary maxima. Chen, Livio, & Gehrels (1993) were the first to suggest that this phenomenon represents an intrinsic physical process which characterizes the outbursts. They proposed that the glitches and bumps are caused by mass transfer events from the companion star, in response to the X-ray heating during the main outburst. They correctly predicted the short orbital period of XN 0422+32 from its early onset of the glitch observed in the UV (Fig. 21). But their model cannot explain the series of mini-outbursts observed in XN 0422 (Fig. 10). A similar model was suggested by Augusteijn, Kuulkers, & Shaham (1993), with a mathematical formulation for the “echoing” of the initial outburst. The latter model has been successful in predicting the equal spacings between the onset of the mini-outbursts in XN 0422, but it has failed to account for the large amplitude of these events. Mineshige (1994), on the other hand, showed

that the secondary maxima could in principle be caused by a thermal instability in the disk, if the disk is moderately irradiated by X-rays, although there is no mechanism for the distinction between glitches, bumps and mini-outbursts, nor for the time delay between these events and the main peak. Recently, Kim et al. (see Wheeler 1996) proposed that the secondary maxima are due to the “stagnation” effect in an indirectly irradiated disk.

While none of the above models can give satisfactory explanations for all the observed features of the secondary maxima, it is worth noting that all the models involve X-ray irradiation of either the companion star or the accretion disk. Therefore, a better understanding of the relationship between the disk X-ray emission and the response of the disk and companion star to irradiation is clearly needed.

One should also keep in mind that the bump shown in the 1–37 keV light curve of XN 1124-683 (Fig. 9) is completely due to an X-ray spectral transition when the rise in the 9–37 keV flux starts to dominate the total flux. This apparently has nothing to do with any of the models just mentioned. The bump shown in the 3-6 keV light curve of XN 0620-00 (Fig. 20), on the other hand, is probably the result of some kind of X-ray irradiation because there is also a similar optical feature (Fig. 20) which appeared several days before the X-ray bump (Chen, Livio, & Gehrels 1993).

*Recurrence times.* In general, the DTI model predicts that the total accreted mass during an outburst,  $\Delta M$ , is related to the outburst recurrence time,  $T_{\text{rec}}$  and the mass overflow rate from the companion star,  $\dot{M}_c$ , through a simple expression,

$$\dot{M}_c \sim \frac{\Delta M}{T_{\text{rec}}}. \quad (5)$$

Therefore, using  $\Delta M$  in Table 9 and  $T_{\text{rec}}$  inferred from Table 7, we can derive  $\dot{M}_c$  for sources with sufficient data. The results are listed in Table 12. These values agree reasonably well with those derived by van Paradijs (1996). For comparison, for sources with known binary period and companion mass, we also list the theoretical mass transfer rates predicted by King et al. (1996) in their binary evolution theory. We see that in all the cases except XN 1456-32 the two values agree reasonably well. An important point is that according to van Paradijs (1996), for a given binary period the mass transfer rate from the companion has to be smaller than some critical value for the source to be a transient. The large mass transfer rate (partly due to an uncertainty in its distance) inferred for XN 1630-472 thus probably indicates a very unusual system with a very large orbital period ( $> 12$  days).

## 8. SUMMARY AND CONCLUSIONS

In this work, we studied the properties of X-ray and optical light curves of X-ray novae. Our collection of XN light curves, although not complete, demonstrates both the striking universality and the rich variability of the long term time profiles of the XN outbursts. First, we have attempted to classify the morphologies observed in the light curves, and in particular identified the following general classes: (1) fast rise and exponential decay (FRED); (2) triangulars; (3) plateaus (long and short); (4) variable decay, and (5) multi-peaks. Only very few outbursts cannot be classified in any of these categories. In addition to the global morphologies, we have identified other light curve features, such as precursors and secondary maxima (the latter of which include “glitches”, “bumps”, and mini-outbursts).

We have presented the distributions of (1) rise timescales, (2) peak luminosities, (3) outburst

amplitudes, (4) decay timescales, and (5) total energy radiated during an outburst. From these distributions we see that the rise timescales have a much broader distribution than the decay timescales. The latter are distributed in a narrow range around 30 days for the brightest outbursts, although the distribution has a broad base for fainter outbursts. We have also found that the distribution of peak luminosities in Eddington units has a narrow Gaussian profile, centered around  $0.2L_{\text{Edd}}$ . The outburst amplitude, which is defined as the ratio between the peak luminosity and the quiescent luminosity in the same energy band (0.4–10 keV in our case), was found to have a broad distribution. Contrary to a recent claim by Narayan, Garcia, & McClintock (1997), there is significant overlap between the distribution of the amplitudes of the BHXNs and those of the NSXNs, rather than a clear division. While this in itself should not be taken as evidence against the existence of a BH horizon, this quantity is clearly not the best parameter to demonstrate this effect.

A  $\text{Log(N)} - \text{Log(S)}$  distribution based on all of the events in our study is consistent with a uniform distribution over the Galactic disk plus a power-law component associated with the apparent excess in the Galactic bulge region, as viewed from a vantage point displaced 8.5 kpc from the center. Extrapolation to  $\sim$  mCrab sensitivity threshold levels suggests a few times  $10^2$  XN in the Galaxy – however, this is a lower limit since we may be sampling only the short end of the recurrence-time distribution.

We have argued that the basic properties of the light curves, and in particular the universal exponential decay and the narrow range of its decay constant can be explained in terms of the disk thermal instability model. A few of the properties (e.g., the broad rise timescale distribution) suggest that the inner part of the accretion flow in quiescence may be represented by an ADAF, joining at some transition radius to an outer standard disk. A full theoretical understanding of additional light curve features, such as precursor and secondary maxima will probably require further study of a variety of feedback processes. It seems very plausible, for example, that the secondary maxima are related to X-ray irradiation effects, either of the secondary star or of the accretion disk. Some of the smaller “bumps” may simply represent the effects of spectral evolution at certain phases of the outburst.

Finally, we would like to note that future, more sensitive X-ray sky monitors will be able to both discover XN outbursts earlier, and follow them for longer periods of time. This will certainly lead to an improved characterization of the various light curve features and eventually to more meaningful constraints on theoretical models.

We sincerely thank John Cannizzo, Josh Grindlay, Jan van Paradijs, Jeff McClintock, Jerome Orosz, Craig Wheeler for informative conversations and comments on the manuscript, Paul Callanan, Eugene Churazov, Ken Ebisawa, Marat Gilfanov, Alan Harmon, Louis Kaluzienski, Shunji Kitamoto, Jim Lochner, Jerome Orosz, William Paciesas, Kentaro Terada, and Mark Wagner for providing the original light curve data, and David Palmer for providing the freeware DataThief by Kees Huyser & Jan van der Laan which greatly eased the pain of digitizing data from publications. We are grateful to the referee for pointing out some errors in the original manuscript and for helping us to improve the presentation of the paper. ML acknowledges support from NASA grants NAGW-2678 and GO 4377. This research has made use of data obtained through the High Energy Astrophysics Science Research Archive Center (HEASARC) Online Services, provided by the NASA-Goddard Space Flight Center, and the Simbad database, operated at CDS, Strasbourg, France.

## REFERENCES

- Abramowicz, M. A., Chen, X., Kato, S., Lasota, J.-P., & Regev, O. 1995, *ApJ*, 438, L37
- Aoki, T., et al. 1992, *PASJ*, 44, 641
- Augusteijn, T., Kuulkers, E., & Shaham, J. 1993, *A&A*, 279, L13
- Amnuel, P.R., & Guseinov, O.H. 1979, *Ap.S.S.*, 63, 131
- Bailyn, C.D., & Orosz, J.A. 1995, *ApJ*, 440, L73
- Bailyn, C.D., et al. 1995, *Nature*, 374, 701
- Bailyn, C.D., Orosz, J.A., McClintock, J.E., & Remillard, R.A. 1996, *Nature*, 378, 157
- Barret, D., et al. 1992, *ApJ*, 392, L19
- Barret, D., Motch, C., Pietsch, W., & Voges, W. 1995, *A&A*, 296, 459
- Belloni, T., Hasinger, G., Pietsch, W., Mereghetti, S., Bignami, G.F., Caraveo, P. 1993, *A&A*, 271, 487
- Bradt, H.V., Doxsey, R.E., & Jernigan, J.G. 1979, in *X-ray Astronomy*, ed. W.A. Baity & L.E. Peterson (Oxford: Pergamon), 3
- Asai, K., et al. 1996, *PASJ*, 48, 257
- Bradt, H.V.D., & McClintock, J.E. 1983, *ARA&A*, 21, 13
- Brandt, S., et al. 1992, *A&A*, 254, L39
- Branduardi, G., Ives, J.C., Sanford, P.W., Brinkman, A.C., & Maraschi, L. 1976, *MNRAS*, 175, 47p
- Callanan, P.J., et al. 1995, *ApJ*, 441, 786
- Callanan, P.J., et al. 1996, *ApJ*, 461, 351
- Callanan, P.J., Garcia, M.R., Filippenko, A.V., McLean, I., & Teplitz, H. 1996, *ApJ*, 470, L57
- Canizares, C.R., McClintock, J.E., & Grindlay, J.E. 1980, *ApJ*, 236, L55
- Cannizzo, J.K. 1993, *ApJ*, 419, 318
- Cannizzo, J.K. 1996, *Mem. S.A.It.*, 67, 269
- Cannizzo, J.K., Chen, W., & Livio, M. 1995, *ApJ*, 454, 880 (CCL95)
- Cannizzo, J.K., Ghosh, P., & Wheeler, J.C. 1982, *ApJ*, 260, L83
- Cannizzo, J.K., Wheeler, J.C., & Polidan, R.S. 1986, *ApJ*, 301, 634
- Casares, J., Charles, P.A., & Marsh, T.R. 1995, *MNRAS*, 277, L45
- Casares, J., Charles, P. A., & Naylor, T. 1992, *Nature*, 355, 614
- Casares, J., Charles, P.A., Jones, D. H.P., Rutten, R.G.M., & Callanan, P.J. 1991, *MNRAS*, 250, 712
- Charles, P.A., et al. 1980, *ApJ*, 237, 154
- Chen, W., Gehrels, N., & Cheng, F.H. 1993, *ApJ*, 403, L71
- Chen, W., Livio, M., & Gehrels, N. 1993, *ApJ*, 408, L5
- Cheng, F.H., Horne, K., Panagia, N., Shrader, C.R., Gilmozzi, R., Parasce, F., & Lund, N. 1992, *ApJ*, 396, 664
- Chevalier, C., & Ilovaisky, S.A. 1990, *A&A*, 238, 163
- Chodil, G., Mark, H., Rodrigues, R., & Swift, C.D. 1968, *ApJ*, 152, L45

- Cominsky, L., Jones, C., Forman, W., & Tananbaum, H. 1978, *ApJ*, 224, 46
- Conner, J.P., Evans, W.D., & Belian, R.D. 1969, *ApJ*, 157, L157
- Cowley, A.P. 1992, *ARA&A*, 30, 287
- Czerny, M., Czerny, B., & Grindlay, J.E. 1987, *ApJ*, 312, 122
- Davis, R.J., Edwards, M.R., Morison, I., & Spencer, R.E. 1975, *Nature*, 257, 659
- Della Valle, M. & Benetti, S. 1993, *IAUC* 5890
- Della Valle, M., Jarvis, B. J., & West, R.M. 1991, *A&A*, 247, L33
- Della Valle, M., Mirabel, I.F., & Rodriguez, L.F. 1994, *A&A*, 290, 803
- Eachus, L.J., Wright, E.L., & Liller, W. 1976, *ApJ*, 203, L17
- Ebisawa, K., et al. 1994, *PASJ*, 46, 375
- Elvis, M., Page, C.G., Pounds, K. A., Ricketts, M.J., & Turner, M.J.L. 1975, *Nature*, 257, 656
- Evans, W.D., Belian, R.D., & Conner, J.P. 1970, *ApJ*, 159, L57
- Eyles, C.J., Skinner, G.K., Willmore, A. P., & Rosenberg, F.D. 1975, *Nature*, 257, 291
- Faulkner, J., Lin, D.N.C., & Papaloizou, J. 1983, *MNRAS*, 205, 359
- Forman, W., Jones, C., & Tananbaum, H. 1976, *ApJ*, 206, L29
- Gontikakis, C., & Hameury, J.-M. 1993, *A&A*, 271, 118
- Grader, R.J., Hill, R.W., Seward, F.D., & Torr, A. 1966, *Science*, 152, 1499
- Greiner, J., Hasinger, G., Molendi, S., & Ebisawa, K. 1994, *A&A*, 285, 509
- Grindlay, J.E., & Gursky, H. 1977, *ApJ*, 218, L117
- Hameury, J.-M., King, A.R., & Lasota, J.-P. 1986, *A&A*, 162, 71
- Hameury, J.-M., King, A.R., & Lasota, J.-P. 1990, *ApJ*, 353, 585
- Harmon, B.A., & Paciesas, W.S. 1993, *IAUC* 5913
- Harmon, B.A., Zhang, S.N., Wilson, C. A., Rubin, B.C., Fishman, G.J., & Paciesas, W.S. 1994, in *The Second Compton Symposium*, ed. C. E. Fichtel, N. Gehrels, & J.P. Norris (New York: AIP), 210
- Harmon, B.A., et al. 1995, *Nature*, 374, 703
- Harries, J.R., McCracken, K.G., Francey, R.J., & Fenton, A.G. 1967, *Nature*, 215, 38
- Haswell, C.A., Robinson, E.L., Horne, K., Stiening, R.F., & Abbott, T.M.C. 1993, *ApJ*, 411, 802
- Hjellming, R.M., & Rupen, M.P. 1995, *Nature*, 375, 464
- Hjellming, R.M., Rupen, M.P., Shrader, C.R., Campbell–Wilson, D., & McKay, D.J., 1996, *ApJ*, 470L, 105.
- Holt, S.S., & Kaluzienski, L.J. 1979, *IAUC* 3342
- Huang, M., & Wheeler, J.C. 1989, *ApJ*, 343, 229
- Ichikawa, S., Mineshige, S., Kato, T. 1994, *ApJ*, 435, 748
- in 't Zand, J. 1992, Ph.D. thesis, Univ. Utrecht
- Jones, C., Forman, W., Tananbaum, H., & Turner, M.J.L. 1976, *ApJ*, 210, L9
- Hynes, R., et al., 1997, in preparation.
- Kaluzienski, L.J. 1977, Ph.D. thesis, Univ. Maryland

- Kaluzienski, L.J., & Holt, S.S. 1975, IAUC 2859
- Kaluzienski, L.J., & Holt, S.S. 1978, IAUC 3144
- Kaluzienski, L.J., Holt, S.S., & Swank, J.H. 1980, ApJ, 241, 779
- Kaluzienski, L.J., et al. 1975, ApJ, 201, L121
- Kaluzienski, L.J., Holt, S.S., Boldt, E.A., & Serlemitsos, P.J. 1977, ApJ, 212, 203
- King, A.R., Kolb, U., & Burderi, L. 1996, ApJ, 464, L127
- Kitamoto, S., et al., 1984, PASJ, 36, 799
- Kitamoto, S., et al. 1989, Nature, 342, 518
- Kitamoto, S., Tsunemi, H., Pedersen, H., Ilovaisky, S.A., & van der Klis, M. 1990, ApJ, 361, 590
- Kitamoto, S., Tsunemi, H., Miyamoto, S., & Roussel-Dupre, D. 1993, ApJ, 403, 315
- Koyama, K., et al. 1981, ApJ, 247, L27
- Laros, J.G., & Wheaton, Wm A. 1980, Nature, 284, 324
- Lasota, J.-P., Narayan, R., & Yi, I. 1996, A&A, 314, 813
- Li, F.K., Sprott, G.F., & Clark, G.W. 1976, ApJ, 203, 187
- Livio, M., & Pringle, J.E. 1992, MNRAS, 259, 23p
- Lochner, J., & Roussel-Dupré, D. 1994, ApJ, 435, 840
- Lloyd, C., Noble, R., & Penston, M.V. 1977, MNRAS, 179, 675
- Maraschi, L., Treves, A., & van den Heuvel, E.P.J. 1976, Nature, 259, 292
- Markert, T.H., et al. 1973, ApJ, 184, L67
- Markert, T.H., et al. 1977, ApJ, 218, 801
- Marsh, T.R., Robinson, E.L., & Wood, J.H. 1994, MNRAS, 266, 137
- Martin, A.C., Casares, J., Charles, P.A., van der Hooft, F., & van Paradijs, J. 1995, MNRAS, 274, L46
- Matilsky, T.A., Giacconi, R., Gursky, H., Kellogg, E.M., & Tananbaum, H.D. 1972, ApJ, 174, L53
- Matsuoka, M., et al. 1980, ApJ, 240, L137
- McClintock, J.E., Horne, K., & Remillard, R.A. 1995, ApJ, 442, 358
- McClintock, J.E., & Remillard, R.A. 1986, ApJ, 308, 110
- McClintock, J.E., & Remillard, R.A. 1990, ApJ, 350, 386
- Mineshige, S. 1994, ApJ, 431, L99
- Mineshige, S., & Wheeler, J.C. 1989, ApJ, 343, 241
- Mineshige, S., Yamasaki, T., & Ishizaka, C. 1993, PASJ, 45, 707
- Mirabel, I.F., & Rodriguez, L.F. 1994, Nature, 371, 46
- Mirabel, I.F., et al. 1994, A&A, 282, L17
- Mitsuda, K., Inoue, H., Nakamura, N., Tanaka, Y. 1989, PASJ, 41, 97
- Moneti, A. 1992, A&A, 260, L7
- Meyer, F., & Meyer-Hofmeister, E. 1984, A&A, 132, 143



- Narayan, R. 1997, in IAU Colloq. 163 on Accretion Phenomena and Related Outflows, ed. D.T. Wickramasinghe, L. Ferrario & G.V. Bicknell (San Francisco: ASP), in press
- Narayan, R., Barret, & McClintock, J.E. 1997, ApJ, in press
- Narayan, R., Garcia, M.R., & McClintock, J.E. 1997, Apj, 478, L79
- Narayan, R., McClintock, J.E., & Yi, I. 1996, ApJ, 457, 821
- Orosz, J.A. 1996, Ph.D. thesis, Yale University
- Orosz, J.A., & Bailyn, C.D. 1995, ApJ, 446, L59
- Orosz, J.A., & Bailyn, C.D. 1997, ApJ, 477, 876
- Orosz, J.A., Bailyn, C.D., Remillard, R.A., McClintock, J.E., & Foltz, C.B. 1994, ApJ, 436, 848
- Orosz, J.A., Bailyn, C.D., McClintock, J.E., & Remillard, R.A. 1996, ApJ, 468, 380
- Orosz, J.A., Remillard, R.A., Bailyn, C.D., & McClintock, J.E. 1997, ApJ, 478, L83
- Paciesas, W.S., et al. 1995, in The Gamma Ray Sky with Compton GRO and SIGMA (Dordrecht: Kluwer), 221
- Paciesas, W.S., Deal, K.J., Harmon, B.A., Zhang, S.N., Wilson, C.A., & Fishman, G.J. 1996, A&AS, 120, 205.
- Parmar, A.N., Angenili, L., & White, N.E. 1995, ApJ, 452, L129
- Parmar, A.N., Stella, L., & White, N.E. 1986, ApJ, 304, 664
- Parmar, A.N., Angenili, L., Roche, P., & White, N.E. 1993, A&A, 279, 179
- Parmar, A.N., White, N.E., Giommi, P., & Gottwald, M. 1986, ApJ, 308, 199
- Parmar, A.N., Williams, O.R., Kuulkers, E., Angelini, L., & White, N.E. 1997, A&A, 319, 855
- Priedhorsky, W.C., & Terrell, J. 1984, ApJ, 280, 661
- Remillard, R.A., McClintock, J.E., & Bailyn, C.D. 1992, ApJ, 399, L145
- Remillard, R.A., McClintock, J. E., Orosz, J.A., & Bailyn, C.D. 1994, BAAS, 26, 1483
- Remillard, R.A., Orosz, J.A., McClintock, J.E., & Bailyn, C.D. 1996, ApJ, 459, 226
- Richter, G.A. 1989, Info. Bull. Var. Stars, No. 3362
- Ricketts, M.J., Pounds, K.A., & Turner, M.J.L. 1975, Nature, 257, 657
- Robinson, C., et al. 1996, ApJ, submitted
- Sanwal, D., et al. 1996, ApJ, 460, 437
- Schmidt, G.D., & Angel, R.P. 1975, IAUC 2843
- Shahbaz, T., Naylor, T., & Charles, P.A. 1994, MNRAS, 268, 756
- Share, et al. 1978, IAUC 3197
- Shrader, C.R., Wagner, R.M., Hjellming, R.M., Han, X.H., & Starrfield, S.G. 1994, ApJ, 434, 698
- Shrader, C.R., Wagner, R.M., Charles, P.A., Harlaftis, E., & Naylor, T. 1997, ApJ, in press
- Sunyaev, R., et al. 1991, ApJ, 383, L49
- Tanaka, Y. 1984, IAUC 3936
- Tanaka, Y. 1993, IAUC 5851

- Tanaka, Y. 1989, in *Two-Topics in X-Ray Astronomy (ESA SP-296)*, ed. J. Hunt & B. Battrock (Paris: ESA), 3
- Tanaka, Y., Makino, F., & Dotani, T. 1991, in *Proceedings of the Workshop on Nova Muscae 1991*, ed. S. Brandt (Lyngby: DSRI), 125
- Tanaka, Y., & Lewin, W.H.G. 1995, in *X-ray Binaries*, ed. W.H.G. Lewin, J. van Paradijs, & E.P.J. van den Heuvel (Cambridge: Cambridge Univ. Press), 126
- Tanaka, Y., & Shibazaki, N. 1996, *ARA&A*, 34, 607
- Terada, K., Miyamoto, S., Kitamoto, S., & Egoshi, W. 1994, *PASJ*, 46, 677
- Tingay, S.J., et al. 1995, *Nature*, 374, 141
- Tsunemi, H., Matsuoka, M., & Takagishi, K. 1977, *ApJ*, 211, L15
- Tsunemi, H., Kitamoto, S., Okamura, S., & Roussel-Dupré, D. 1989, *ApJ*, 337, L81
- van der Woerd, H., White, N.E., & Kahn, S.M. 1989, *ApJ*, 344, 320
- van Paradijs, J. 1995, in *X-ray Binaries*, ed. W.H.G. Lewin, J. van Paradijs, & E.P.J. van den Heuvel (Cambridge: Cambridge Univ. Press), 536 (vP95)
- van Paradijs, J. 1996, *ApJ*, 464, L139
- van Paradijs, J., & McClintock, J.E. 1995, in *X-ray Binaries*, ed. W.H.G. Lewin, J. van Paradijs, & E.P.J. van den Heuvel (Cambridge: Cambridge Univ. Press), 58
- van Paradijs, J., & Verbunt, F. 1984, in *High Energy Transients in Astrophysics (AIP Conf. Proc. 115)*, ed. S.E. Woosley (New York: AIP), 49
- van Paradijs, J., Verbunt, F., Shafer, R.A., & Arnaud, K.A. 1987, *A&A*, 182, 47
- Verbunt, F., Belloni, T., Johnston, H.M., van der Klis, M., & Lewin, W.H.G. 1994, *A&A*, 285, 903
- Vishniac, E.T., & Wheeler, J.C. 1996, *ApJ*, 471, 921
- Wachmann, A.A. 1948, *Erg. Astron. Nachr.*, 11(5), E42
- Wade, R.A., Quintana, H., Horne, K., & Marsh, T. 1985, *PASP*, 97, 1092
- Wagner, R.M., et al. 1991, *ApJ*, 378, 293
- Wagner, R.M., Kreidl, T.J., Howell, S.B., & Starrfield, S.G. 1992, *ApJ*, 401, L97
- Wagner, R.M., Starrfield, S.G., Howell, S.B., Kreidl, T.J., & Hjellming, R.M. 1994, *ApJ*, 429, L25
- Watson, M.G., & Ricketts, M.J. 1978, *MNRAS*, 183, 35p
- Watson, M.G., Ricketts, M.J., & Griffiths, R.E. 1978, *ApJ*, 221, L69
- Wheeler, J.C. 1996, preprint (astro-ph/9606119)
- White, N.E. 1994, in *The Evolution of X-Ray Binaries*, ed. S.S. Holt & C.S. Day (New York: AIP), 53
- White, N.E., & van Paradijs, J. 1996, *ApJ*, 473, L25
- White, N.E., Kaluzienski, J.L., & Swank, J.H. 1984, in *High Energy Transients in Astrophysics (AIP Conf. Proc. 115)*, ed. S.E. Woosley (New York: AIP), 31
- Woosley, S.E. (editor) 1984, *High Energy Transients in Astrophysics* (New York: AIP)
- Zhang, S.N., et al. 1996, *A&AS*, 120, 279

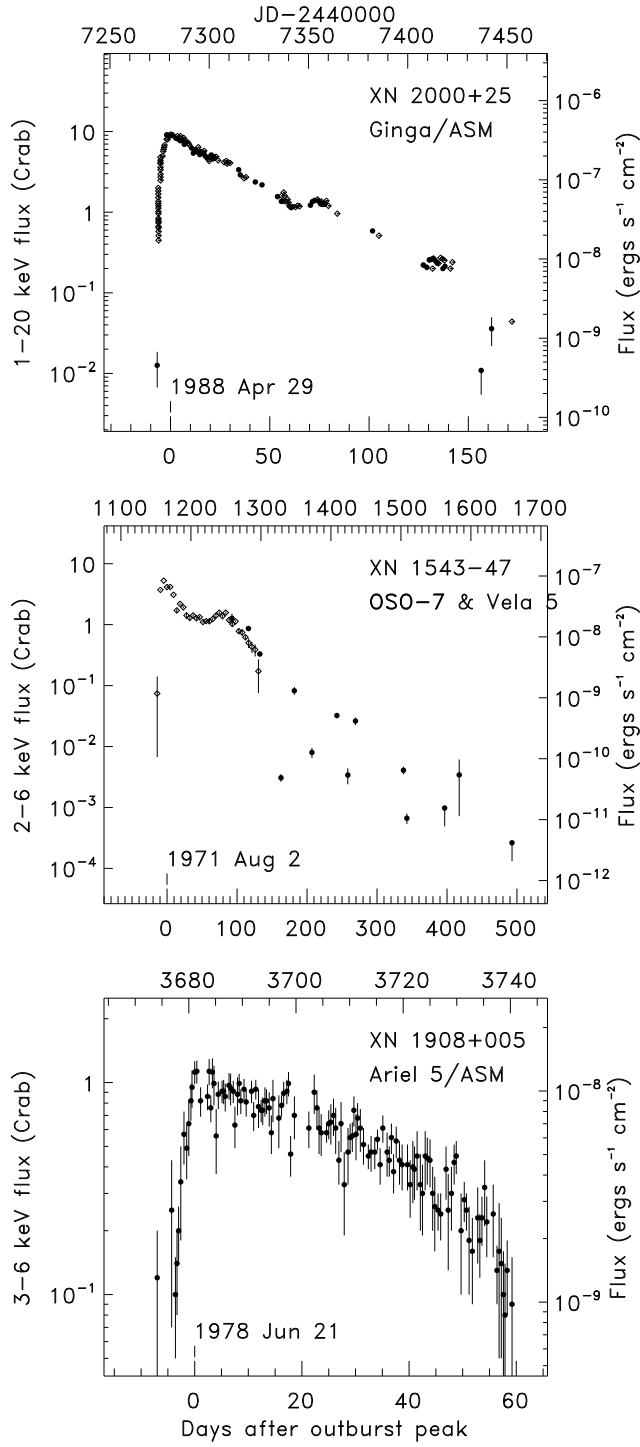


Fig. 1.— Examples of the FRED-type X-ray light curves. (a) The 1988 outburst of GS 2000+25 (Tsunemi et al. 1989), a BH<sub>XN</sub>; (b) the 1974 outburst of 4U 1543–47 (Li et al. 1976), also a BHC; (c) the 1978 outburst of 4U 1908+005 (Charles et al. 1980), a NS<sub>XN</sub>. Note that both (a) and (b) exhibit a ‘glitch’-type secondary maximum (see § 4.3.3).

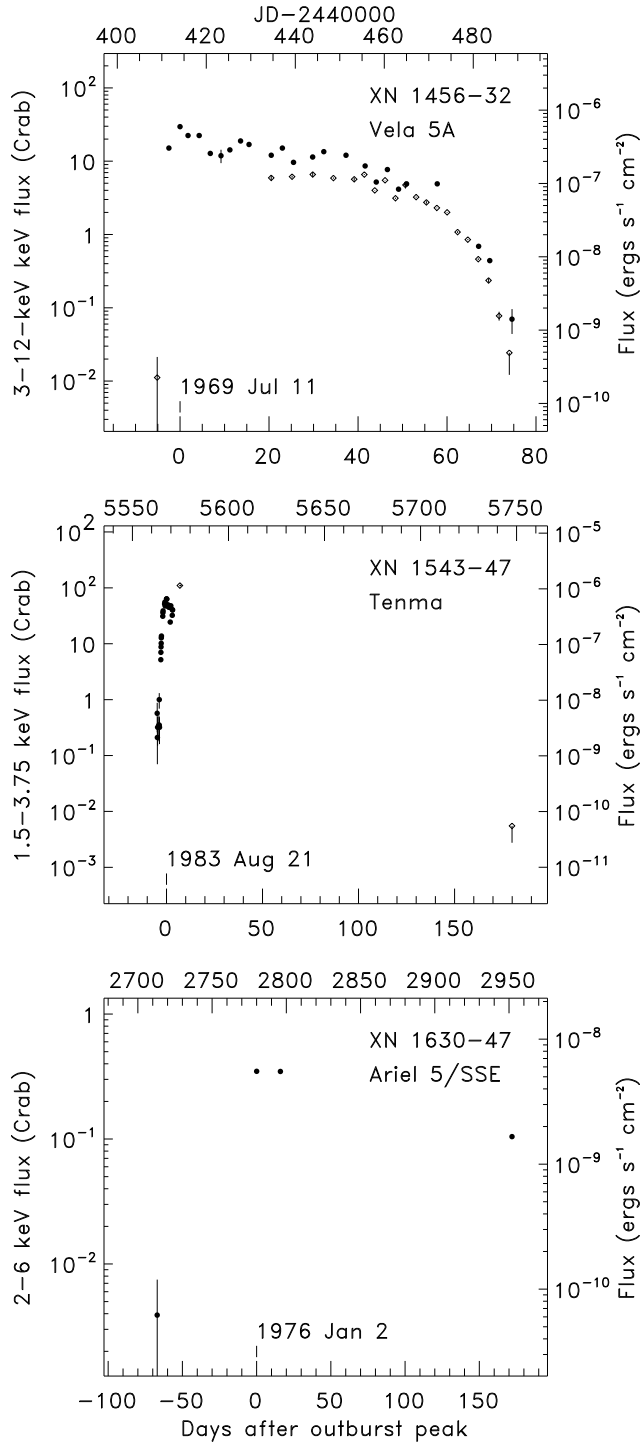


Fig. 2.— Examples of possible FRED light curves. (a) The 1969 outburst of 4U 1456-32 (Evans et al. 1970); (b) the 1983 outburst of 4U 1543-47 (Kitamoto et al. 1984); (c) the 1976 outburst of 4U 1630-472 (Jones et al. 1976).

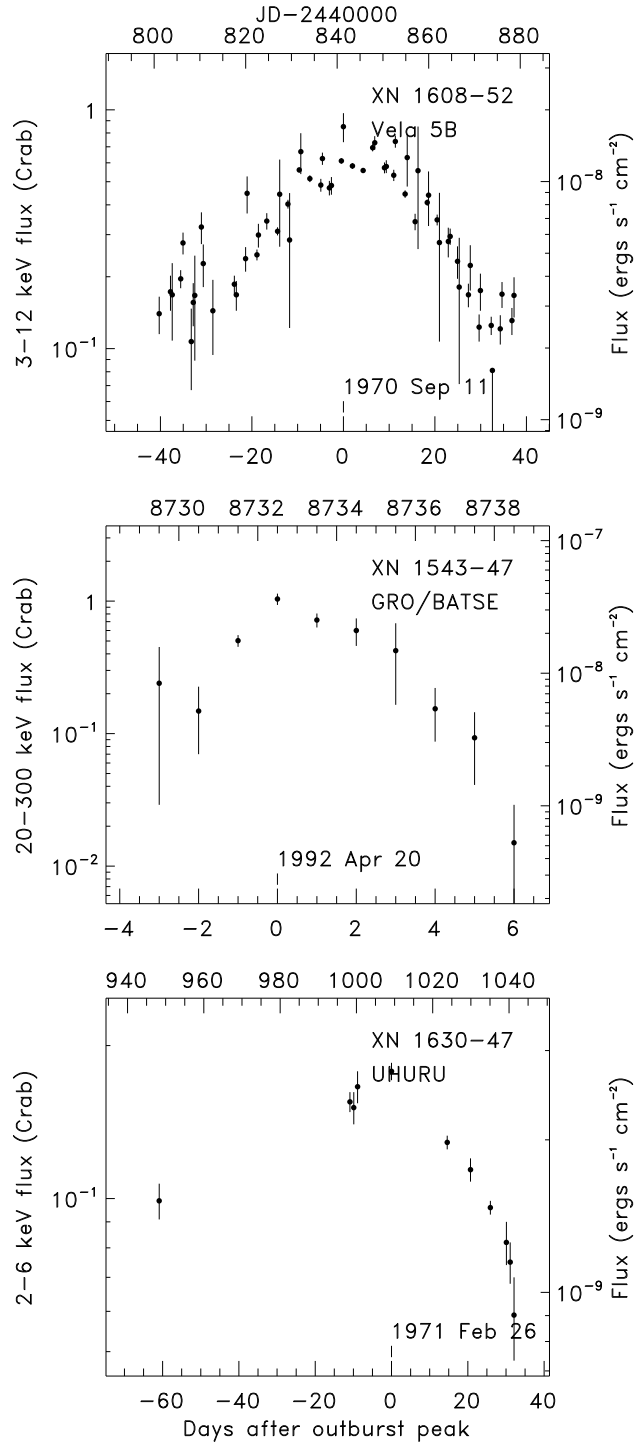


Fig. 3.— Examples of triangular light curves. (a) The 1970 outburst of 4U 1608–52 (Lochner & Roussel-Dupré 1994); (b) the 1992 outburst of A 1543–47 (Harmon et al. 1994) in hard X-rays; (c) the 1971 outburst of 4U 1630–472 (Forman et al. 1976) in which the rise timescale may be longer than the decay timescale.

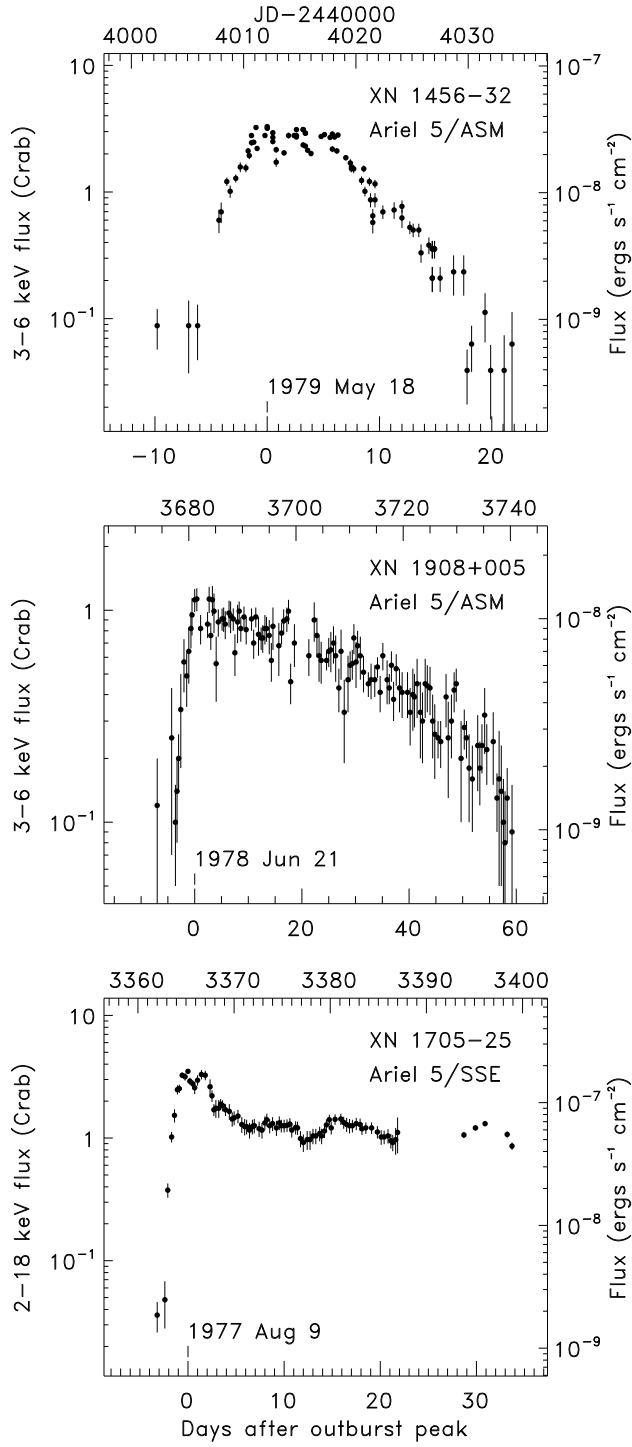


Fig. 4.— Examples of short plateaus which are usually followed by normal decay. (a) The 1979 outburst of 4U 1456–32 (Kaluziński et al. 1980); (b) the 1978 outburst of 4U 1908+005 (Charles et al. 1980); (c) the 1977 outburst of 1H 1705–25 (Griffiths et al. 1978; Share et al. 1978). The late phase of this outburst is uncertain.

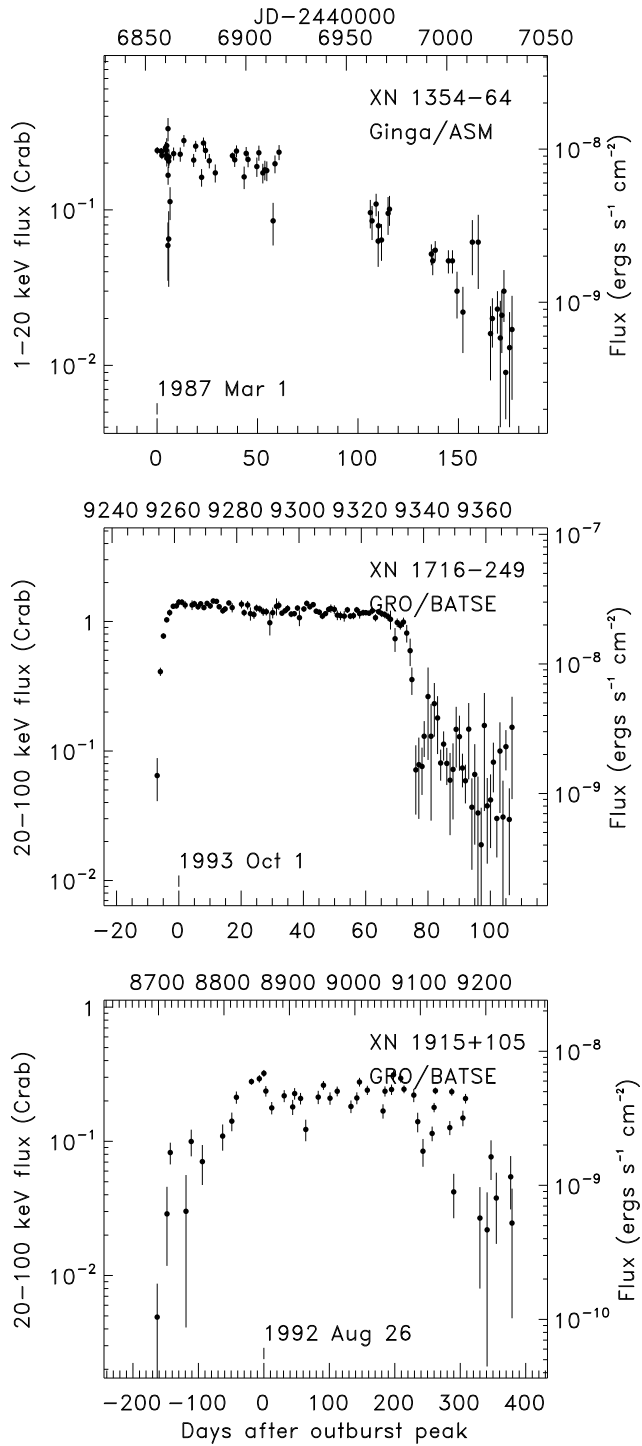


Fig. 5.— Examples of long plateau X-ray light curves. (a) The 1987 outburst of A 1354-64 (Kitamoto et al. 1990), a plateau of 50 days followed by normal decay; (b) the 1993 outburst of GRS 1716-249 (Harmon et al. 1994) which has a fast rise and a sudden cutoff; (c) the 1992 outburst of GRS 1915+105 (Harmon et al. 1994), the longest plateau to date, which has a very slow rise.

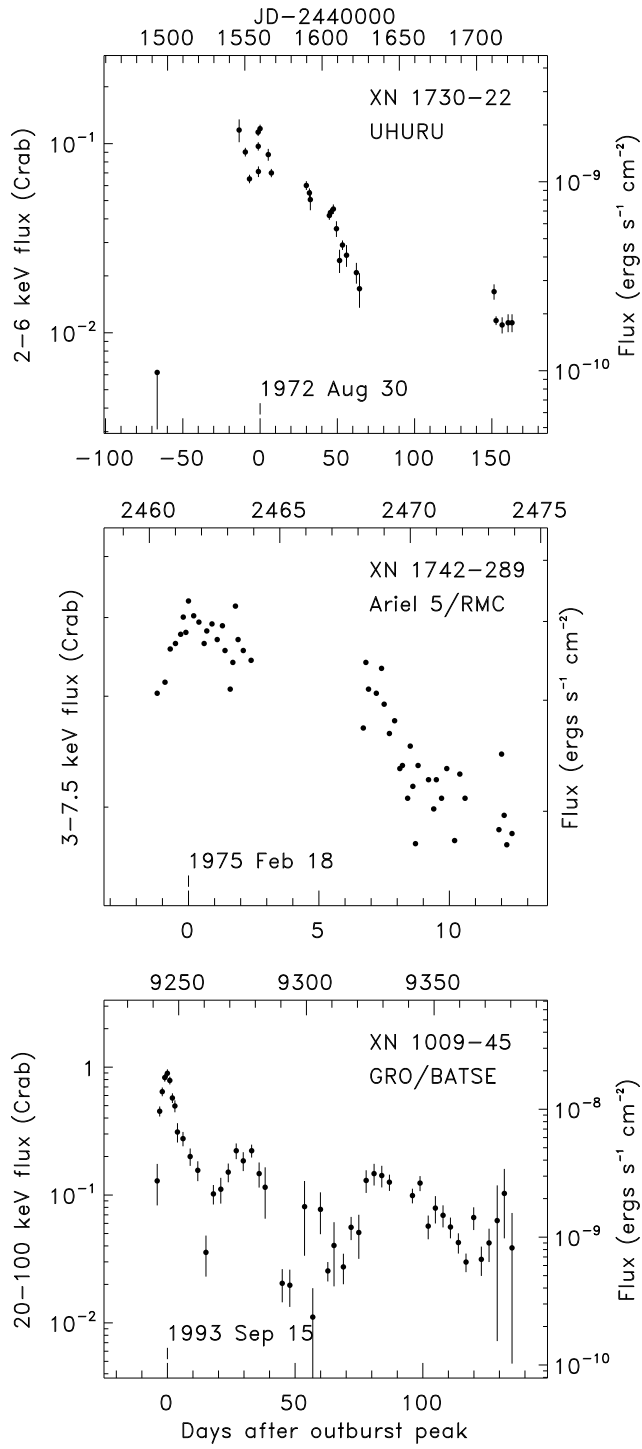


Fig. 6.— Examples of light curves with variable decay constants. (a) The 1972 outburst of 4U 1730-22 (Cominsky et al. 1978); (b) the 1975 outburst of A 1742-289 (Eyles et al. 1975; Branduardi et al. 1976); (c) the 1993 outburst of GRS 1009-45 (Harmon et al. 1994) in hard X-rays.



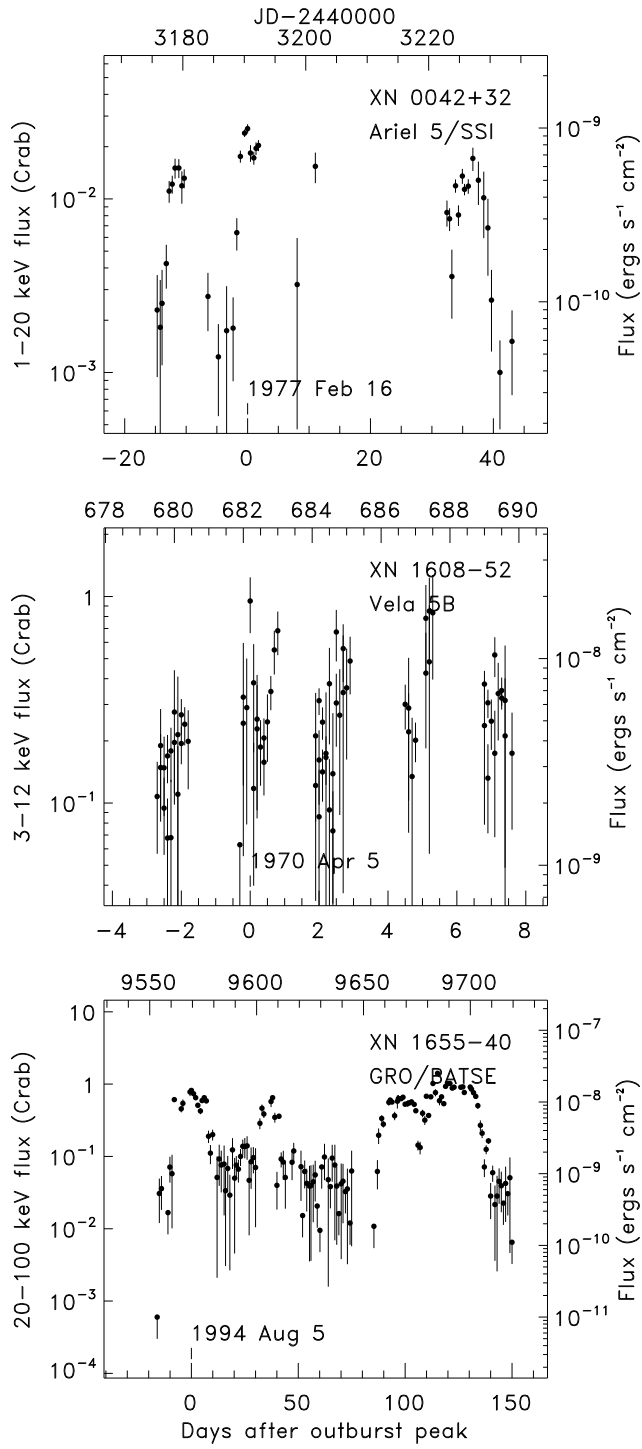


Fig. 7.— Examples of light curves with multiple peaks of comparable strength. (a) The 1977 outburst of 3U 0042+32 (Watson & Ricketts 1978); (b) the 1970 outburst of 4U 1608-52 (Lochner & Roussel-Dupré 1994); (c) the 1994 outburst of GRO J1655-40 (Harmon et al. 1995) in hard X-rays.

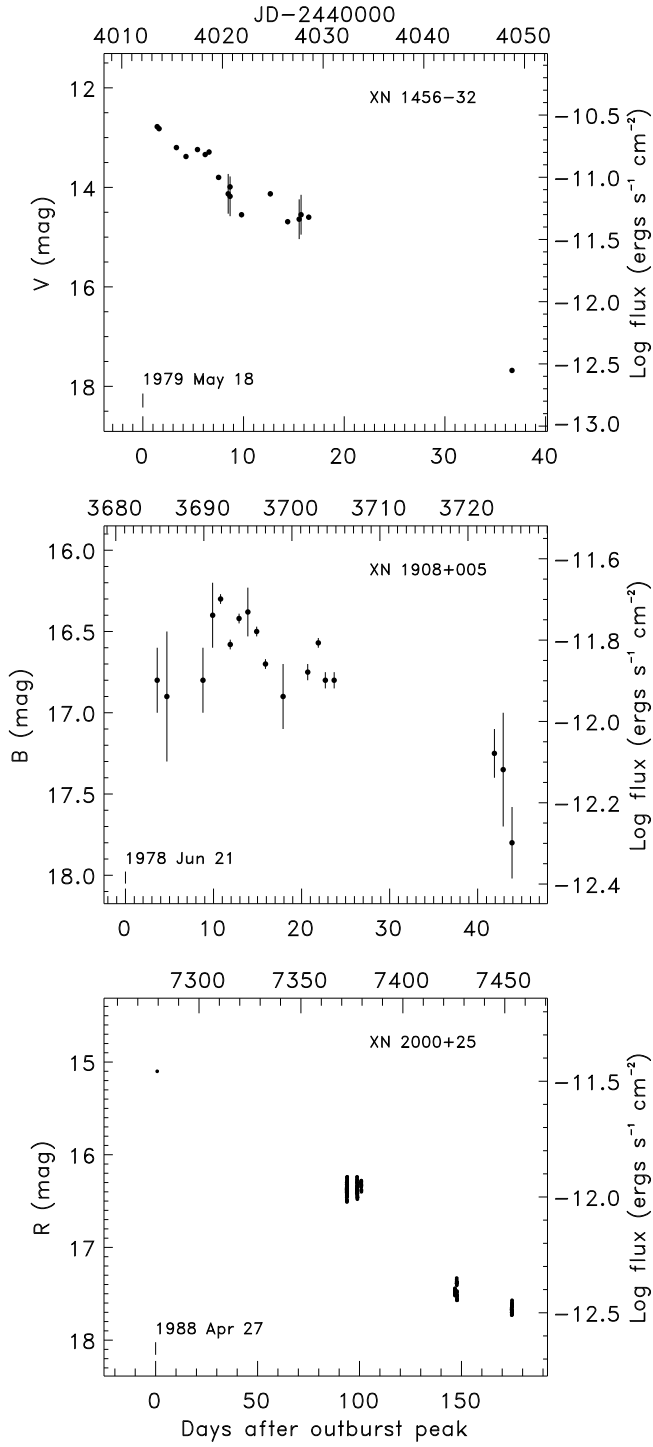


Fig. 8.— Examples of optical light curves. (a) The 1979 outburst of 4U 1456-32 (Canizares, McClintock, & Grindlay 1980); (b) the 1978 outburst of 4U 1908+005 (Charles et al. 1980); (c) the 1988 outburst of GS 2000+25 (Chevalier & Ilovaisky 1990).

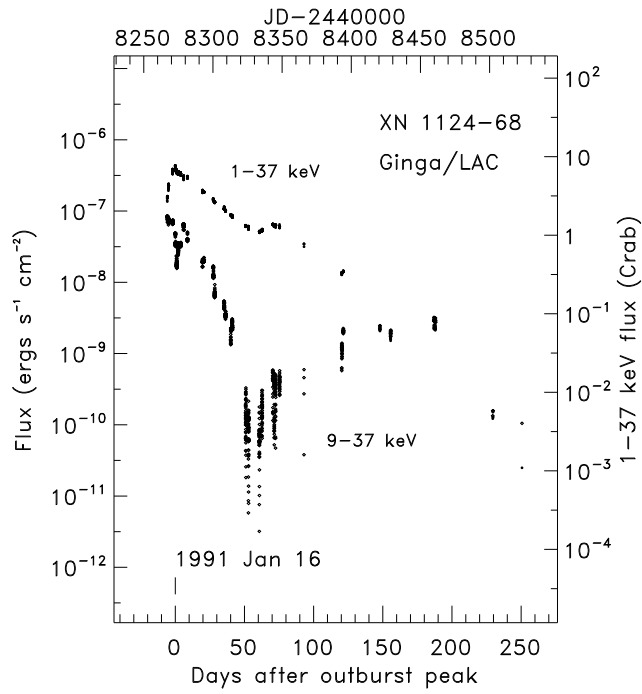


Fig. 9.— The *Ginga* 1-37 keV and 9-37 keV light curves of the 1991 outburst of XN 1124-683 (Ebisawa et al. 1994).

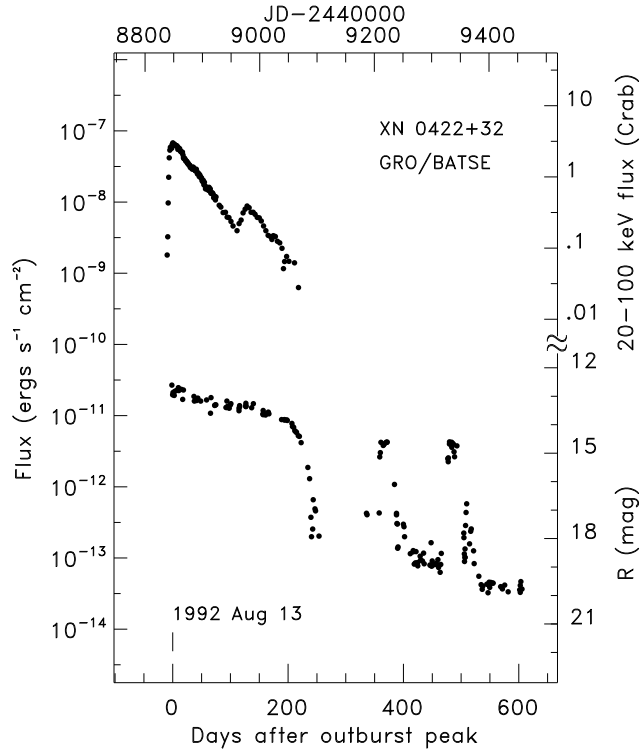


Fig. 10.— The *Compton*/BATSE 20-100 keV X-ray and R-band optical light curves of the 1992 outburst of XN 0422+32 (Pacinas et al. 1995; Callanan et al. 1995).

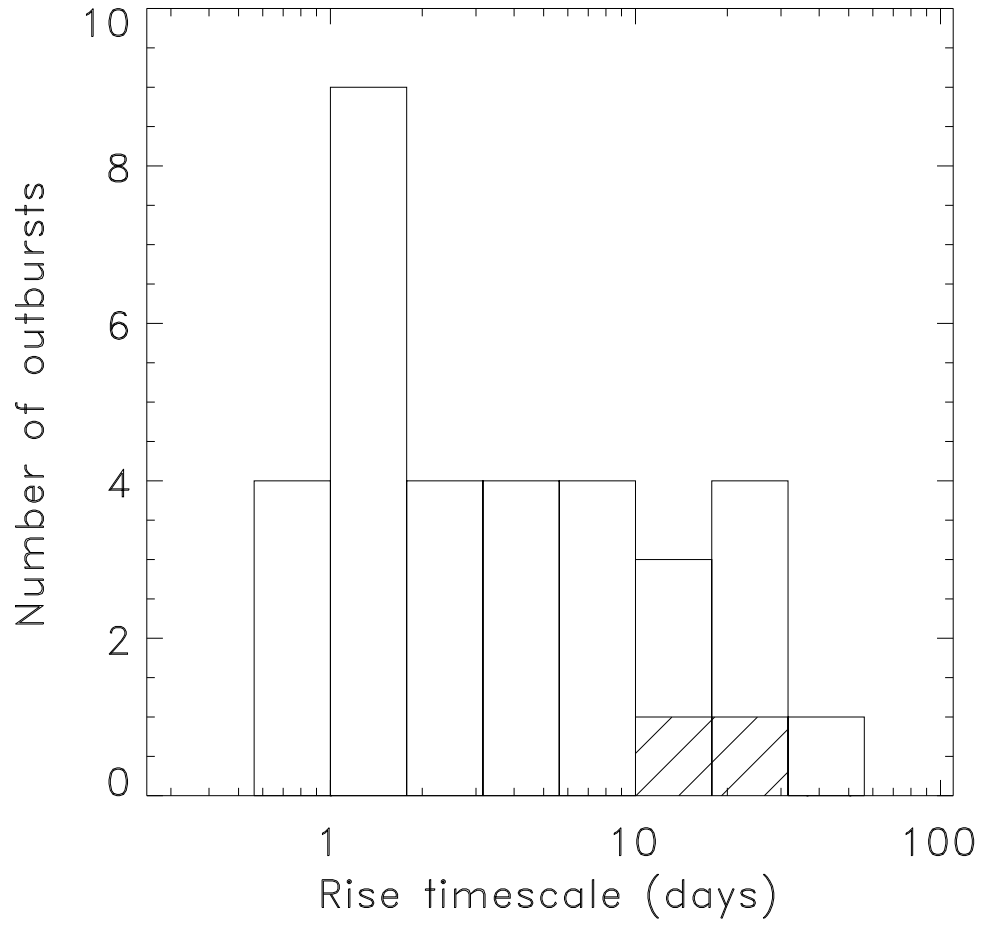


Fig. 11.— The distribution of rise timescales,  $\tau_r$  in logarithmic spacing. The shaded areas are the *upper* limits. Notice the almost flat distribution and the single peak at 1–2 days.

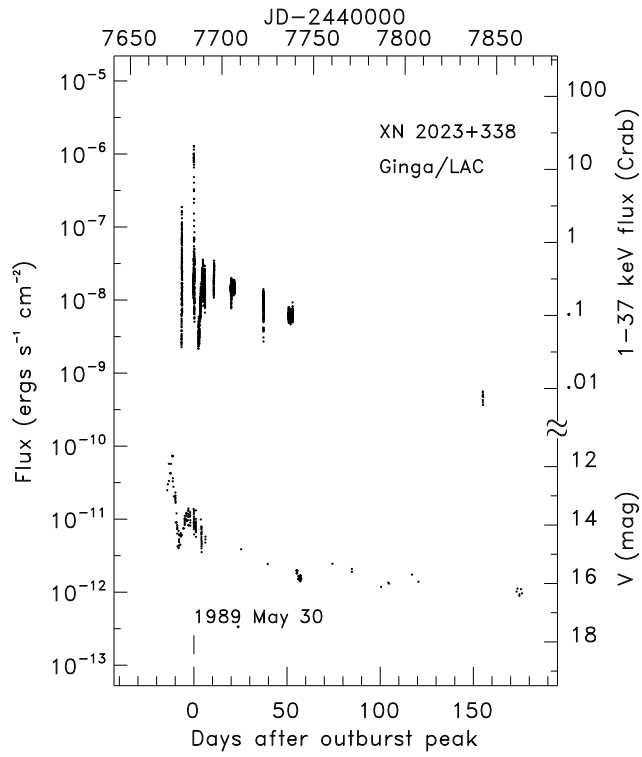


Fig. 12.— The *Ginga*/LAC 1-37 X-ray and V-band optical light curves of XN 2023+338 in 1989. Notice that the optical may have peaked a few days before the X-rays.

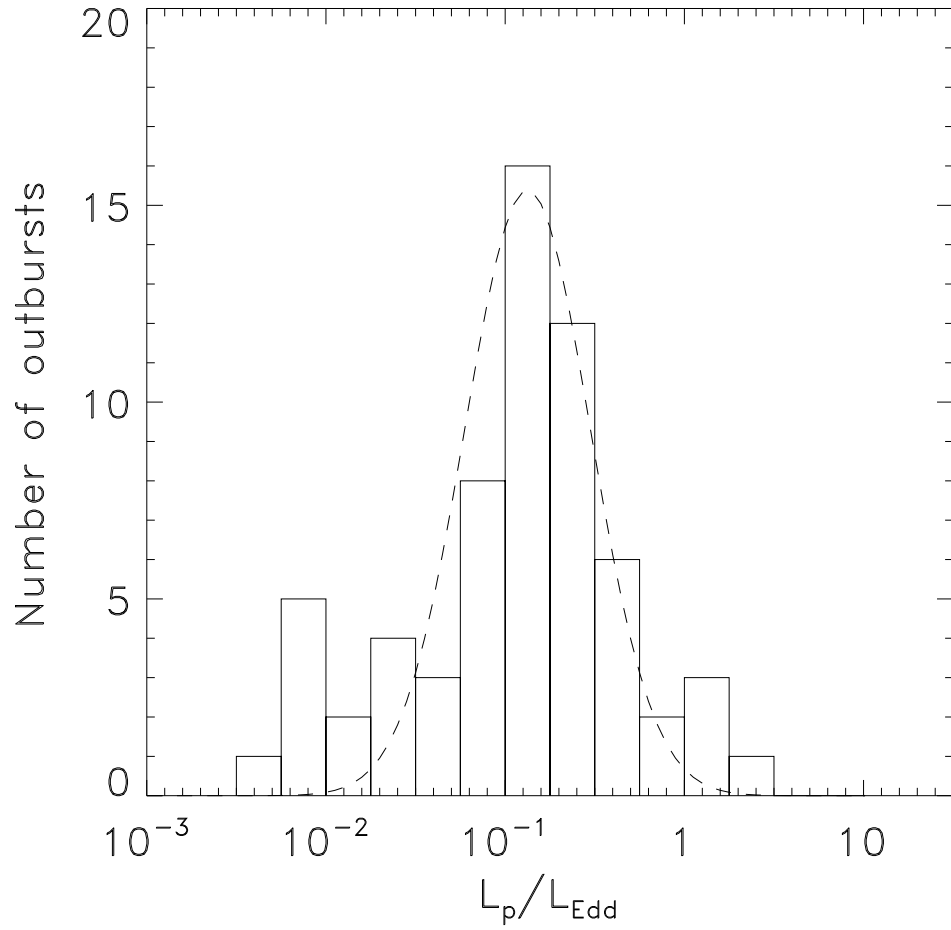


Fig. 13.— The peak luminosity distribution in the units of Eddington limit in logarithmic scale. The dashed line is a Gaussian fit.

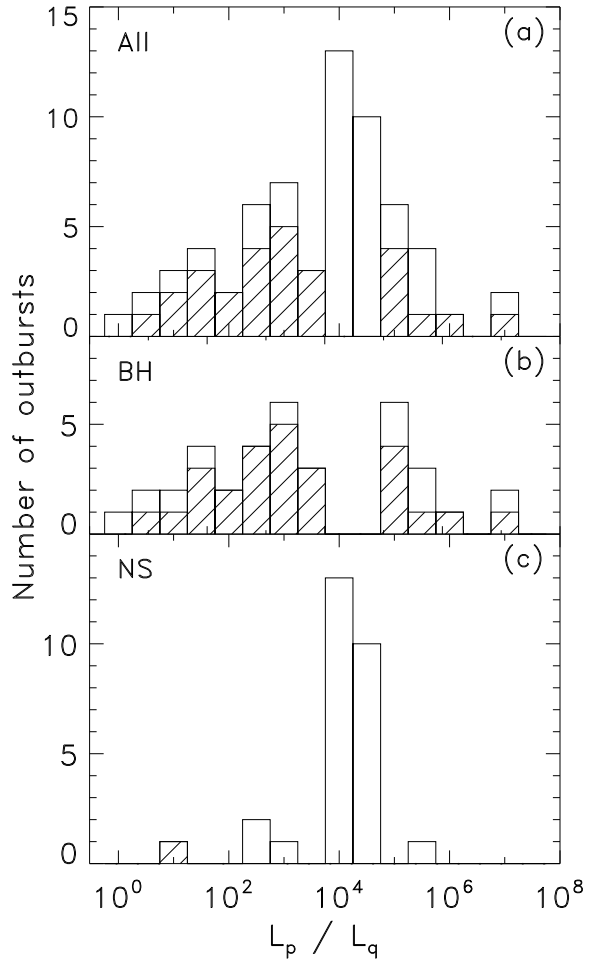


Fig. 14.— The peak amplitude distribution of XN outbursts in logarithmic spacing. (a) All sources, (b) BH events, (c) NS events. The shaded areas are the *lower limits* derived from the peak outburst flux and the upper limits of the quiescent flux.



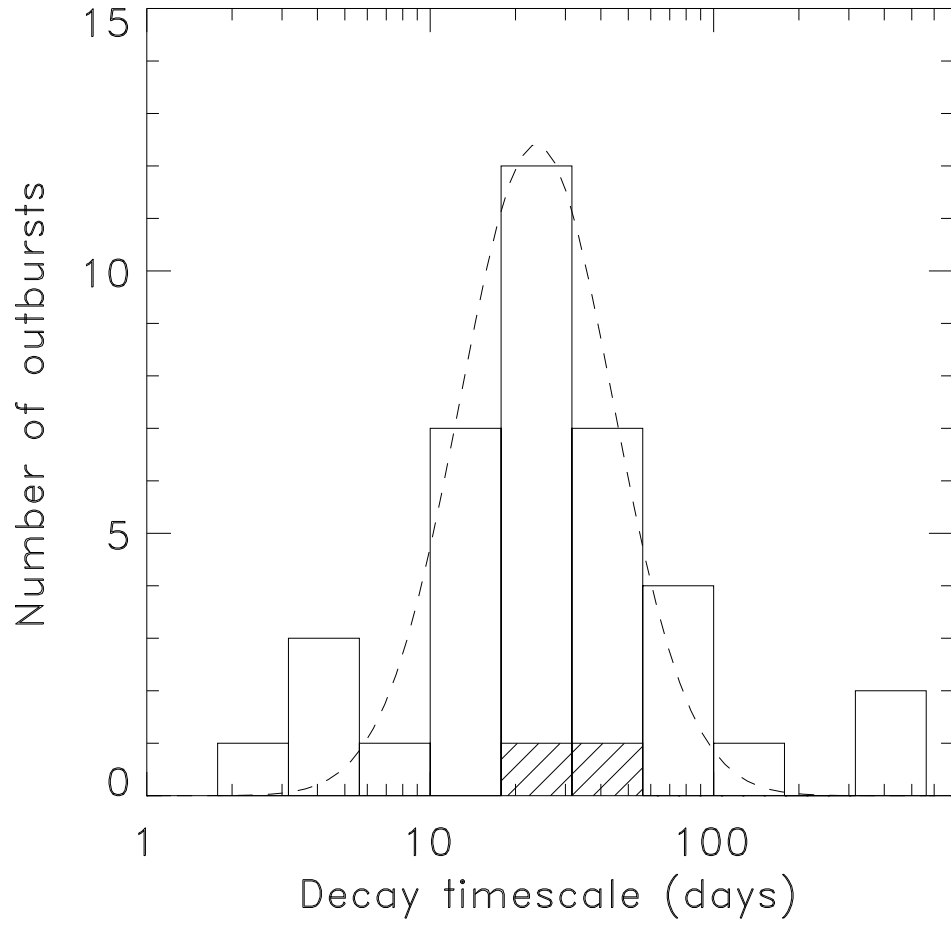


Fig. 15.— The distribution of decay timescales,  $\tau_d$  in logarithmic spacing. The shaded areas are the *upper limits*.

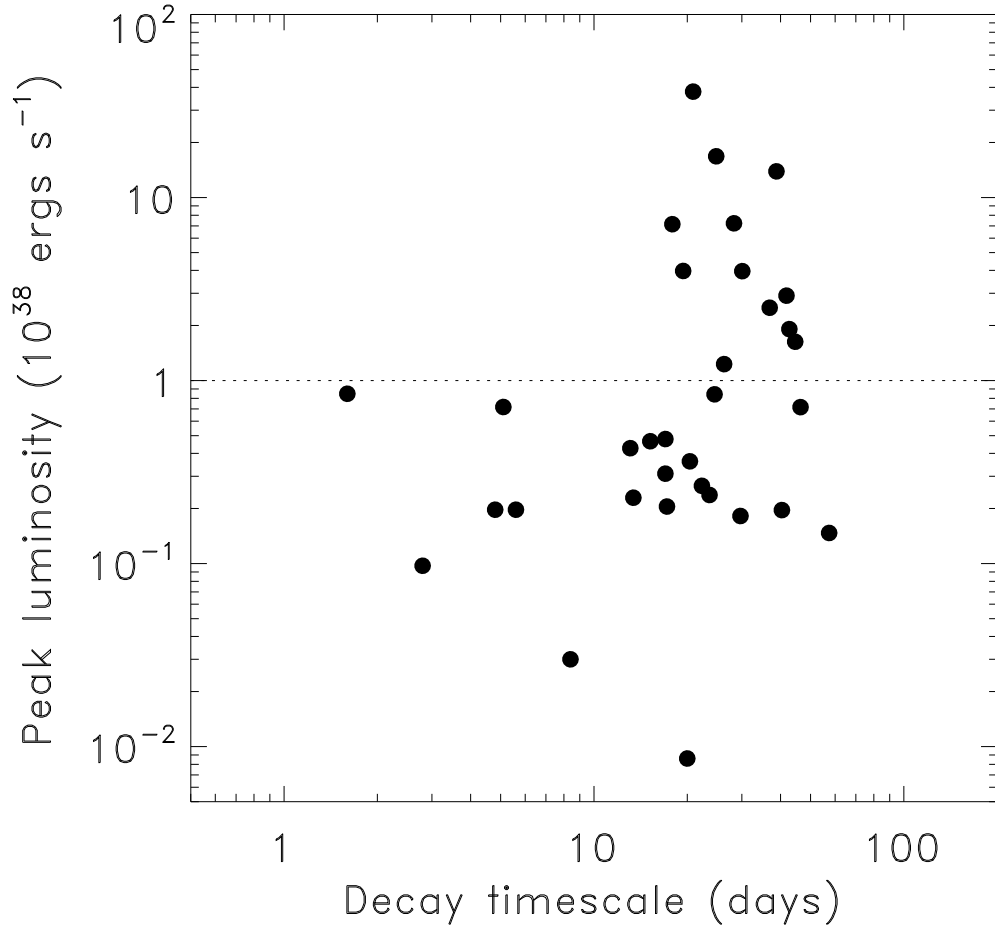


Fig. 16.— The correlation between outburst peak luminosity and decay timescale of the normal outbursts (excluding the plateau events).

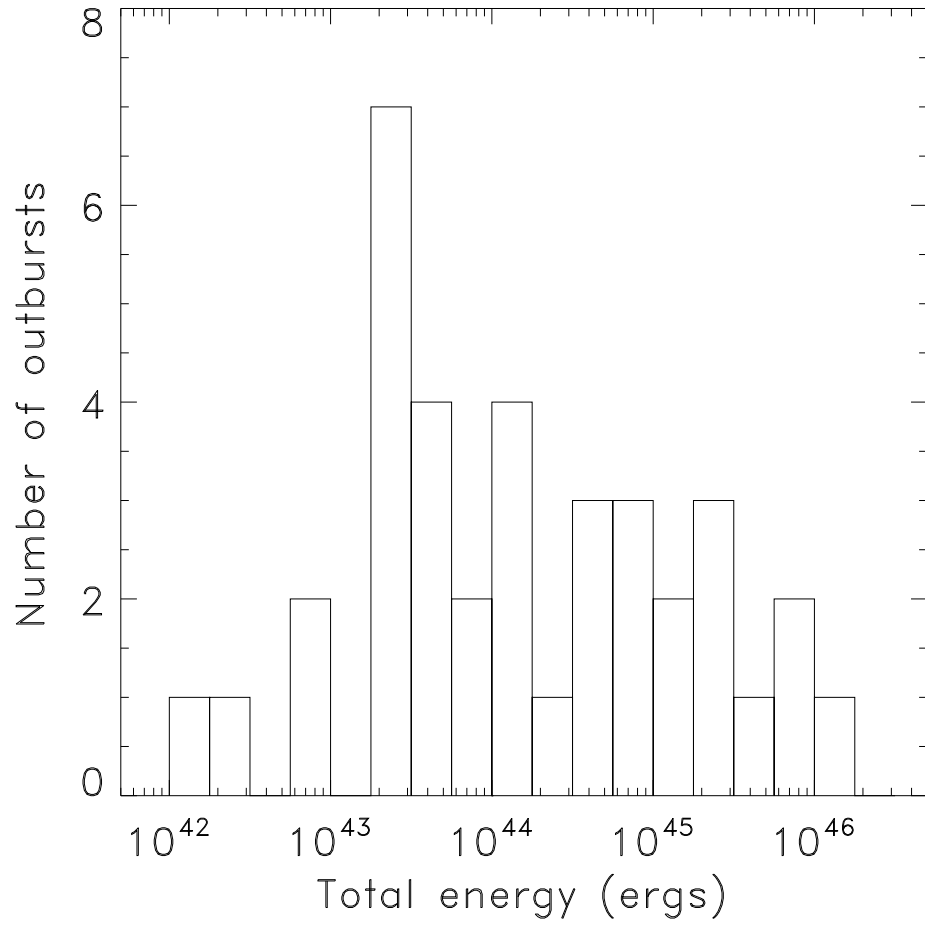


Fig. 17.— The distribution of the total energy radiated in the 0.4-10 keV band during the outburst.

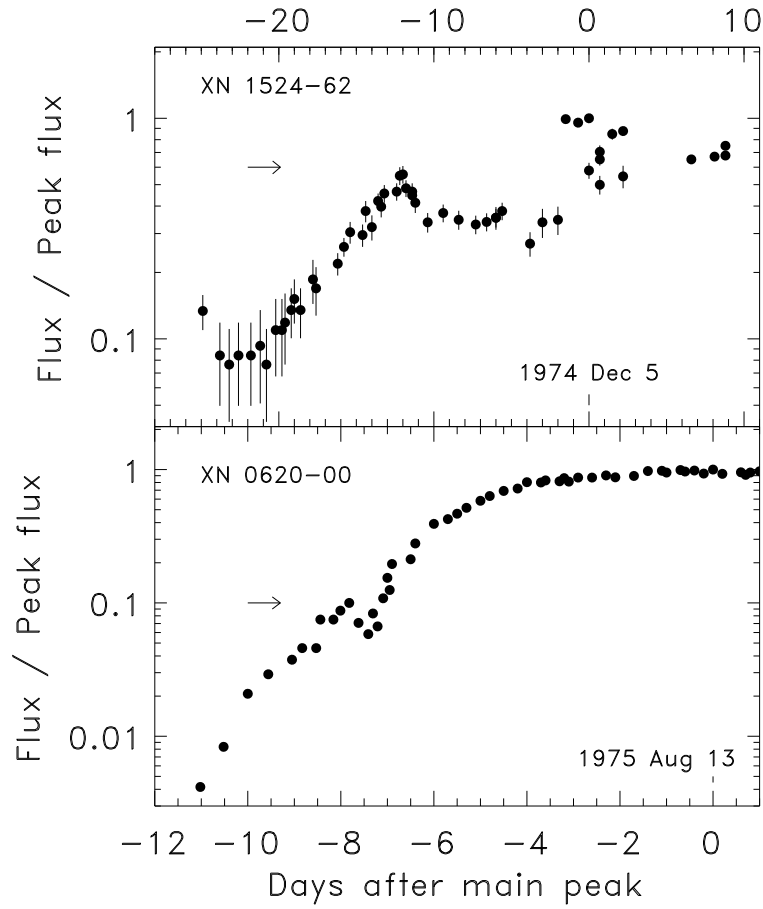


Fig. 18.— The precursor peaks seen in the light curves of (a) XN 1524-62 (Kaluziński et al. 1975) and (b) XN 0620-00 (Elvis et al. 1975). The  $y$ -axis is the ratio of the observed flux to the peak flux. The precursors are marked by the horizontal arrows which are at 60% of the peak flux for XN 1524-62 and 10% for XN 0620-00. Notice that the time span of the *upper* panel is 3 times longer than that of the *lower* panel.

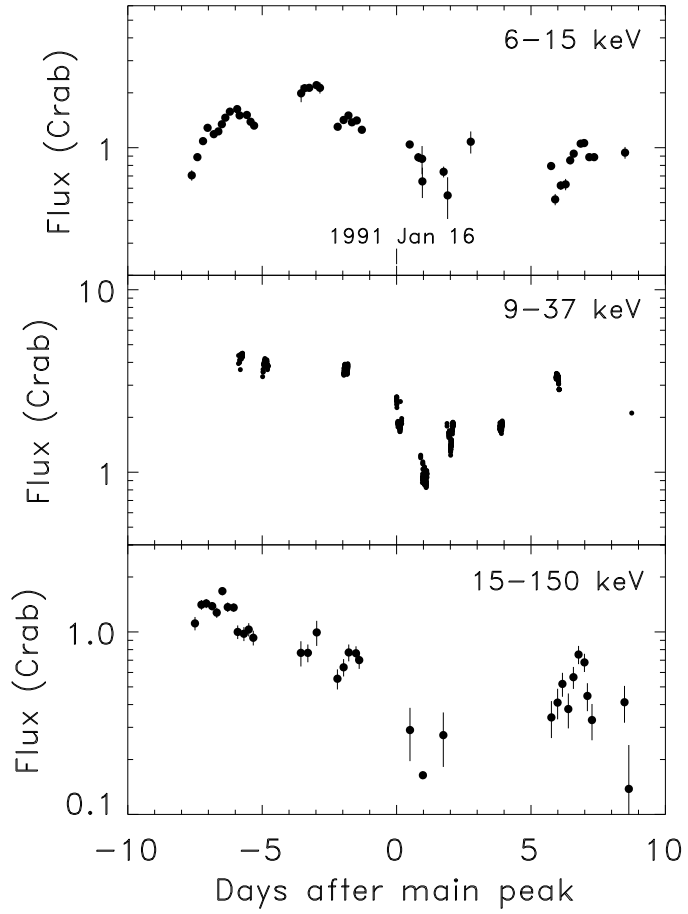


Fig. 19.— High energy light curves of XN 1124–683. The marked peak date at Day 0 is for the *Ginga* light curve in 1–37 keV. The precursor(s) are seen only in (a) the *Granat*/WATCH 6–15 keV (Brandt et al. 1992) and (b) *Ginga*/LAC 9–37 keV light curves (Ebisawa, Ogawa, & Terada 1994), but not clearly in (c) the WATCH 15–150 keV light curve (Brandt et al. 1992).

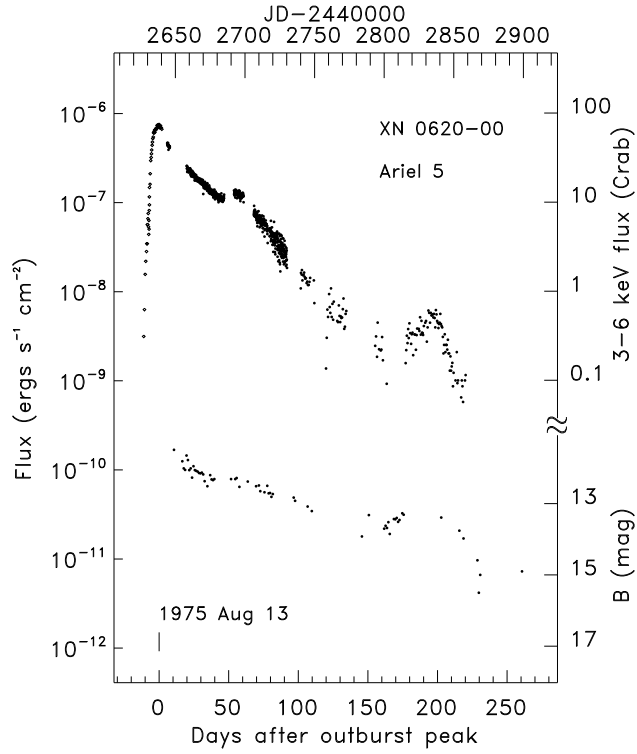


Fig. 20.— The *Ariel 5* 3-6 keV X-ray and B-band optical light curves of the 1975 outburst of XN 0620-00 (Kaluziński et al. 1977; Elvis et al. 1975; Tsunemi et al. 1977).

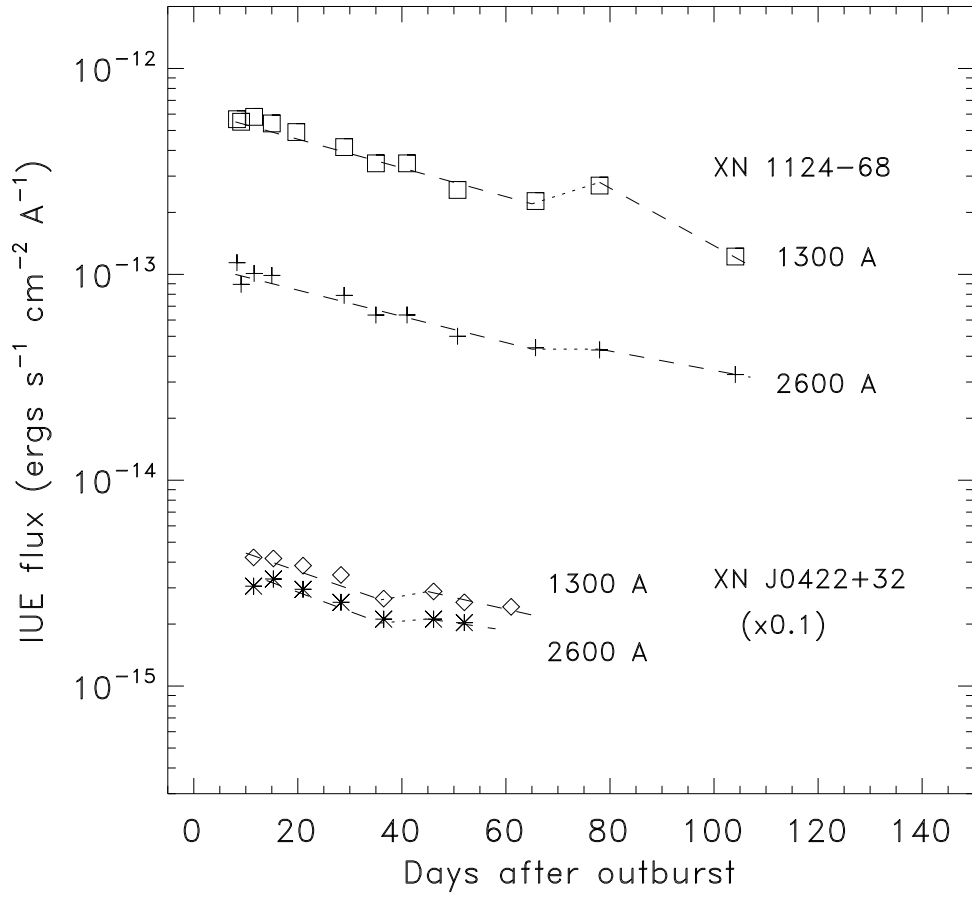


Fig. 21.— The *IUE* UV light curves of the 1991 outburst of XN 1124-683 and 1992 outburst of XN J0422+32 (Shrader & Gonzalez-Riestra 1991; Shrader et al. 1994).

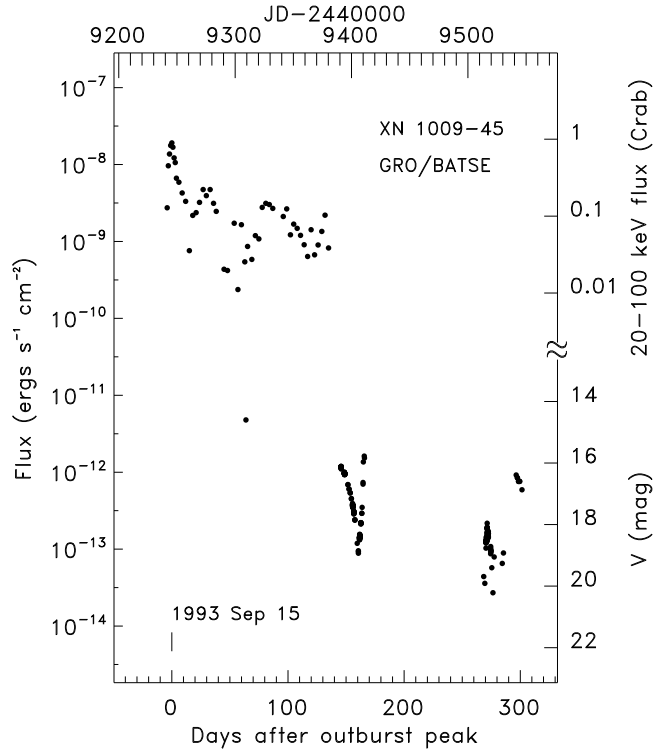


Fig. 22.— The *Compton*/BATSE 20-100 keV hard X-ray and V-band optical light curves of the 1993 outburst of XN 1009-45 (Paciesas et al. 1995; Bailyn & Orosz 1995).



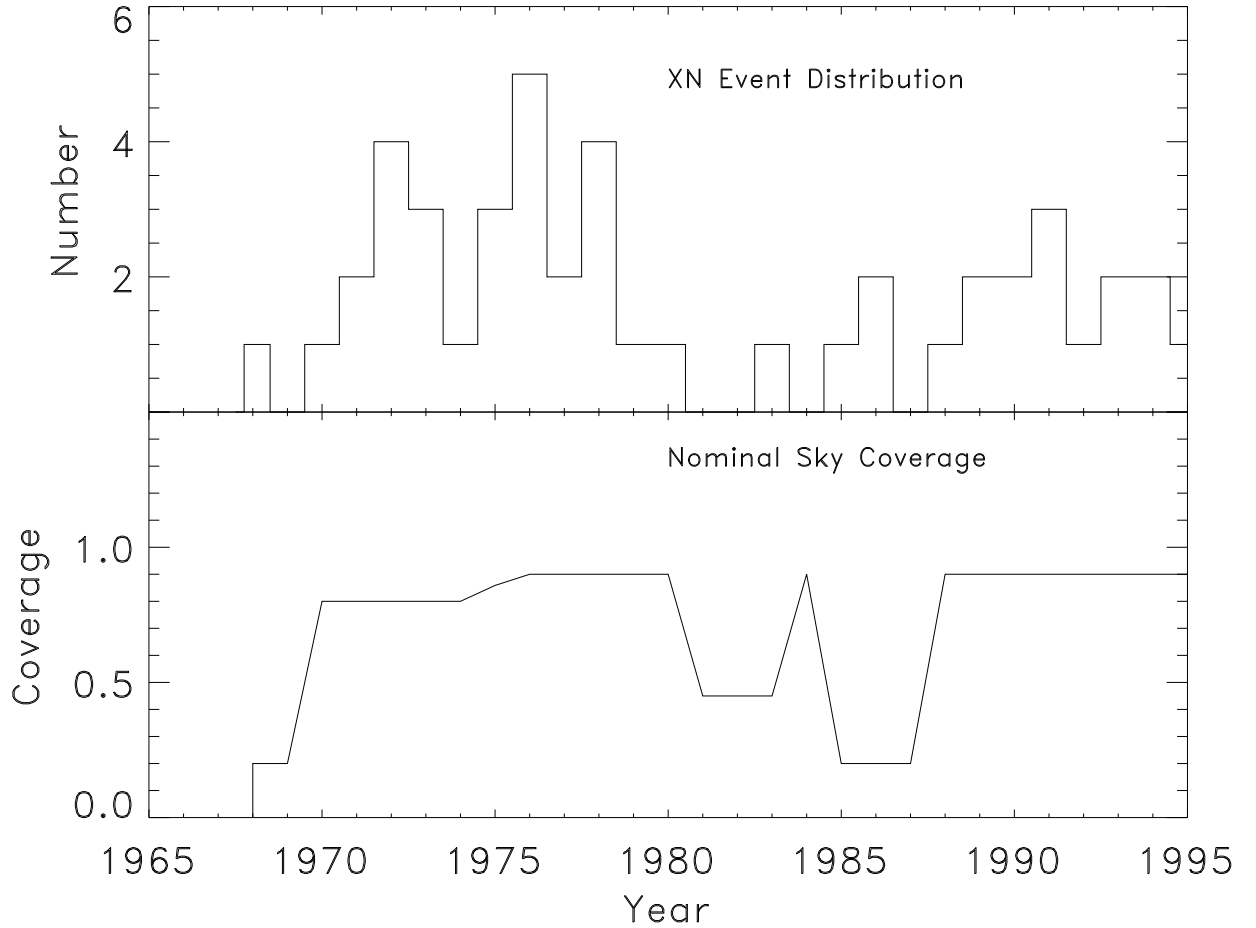


Fig. 23.— (*Upper panel*): Histogram of the XN events per year from 1965 to 1995. (*Lower panel*): Nominal sky coverage factor over the same period. Since we include only events which lasted more than 10 days, any scanning instruments which can cover the whole sky within a few days are considered to provide a sky coverage fraction of close to unity. Notice the period around 1985 with very low sky coverage and the corresponding low event rate. Notice also the low event rate in early 1980's when the sky coverage was adequate.

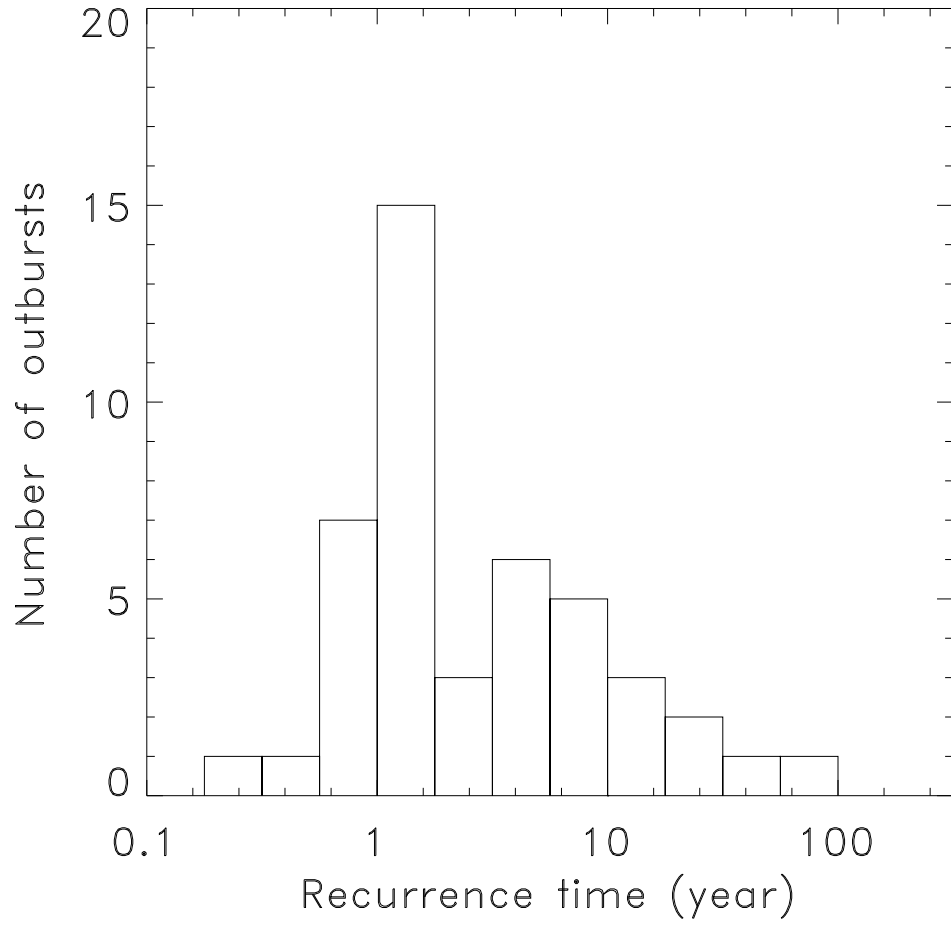


Fig. 24.— The distribution of the recurrence times between outbursts.

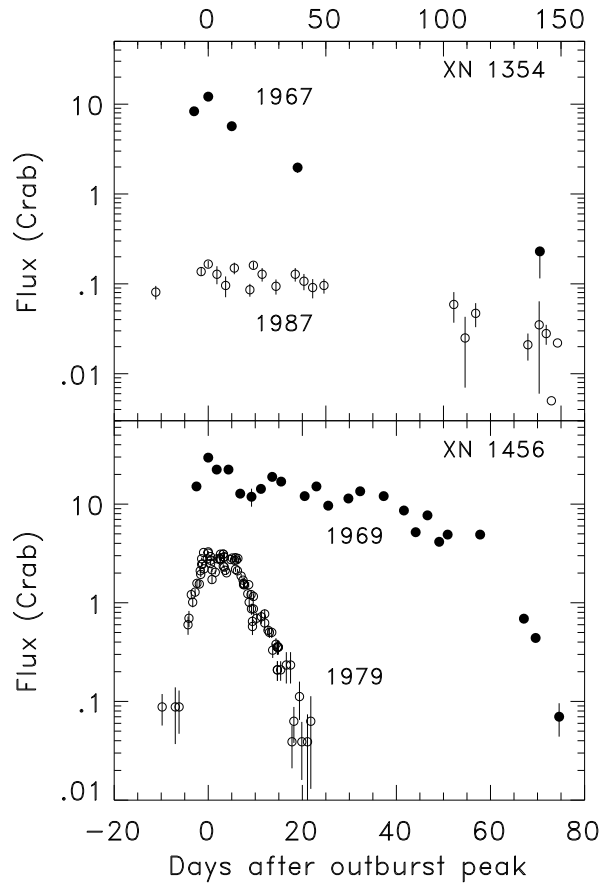


Fig. 25.— Comparison between the major and minor outbursts in XN 1354–64 (Cen X-2, Chodil et al. 1968; Kitamoto et al. 1990) and XN 1456–32 (Cen X-4, Conner, Evans, & Belian 1969; Evans, Belian, & Conner 1970; Kaluziński et al. 1980). The two major outbursts from the two sources are about the same peak intensity, but their two minor ones differ by more than a factor of 10. Notice the changing of shapes and durations from the major to the minor outbursts. Also notice that the time span of the upper panel is 2 times that of the lower panel.

## Galactic Distribution of X-Ray Novae

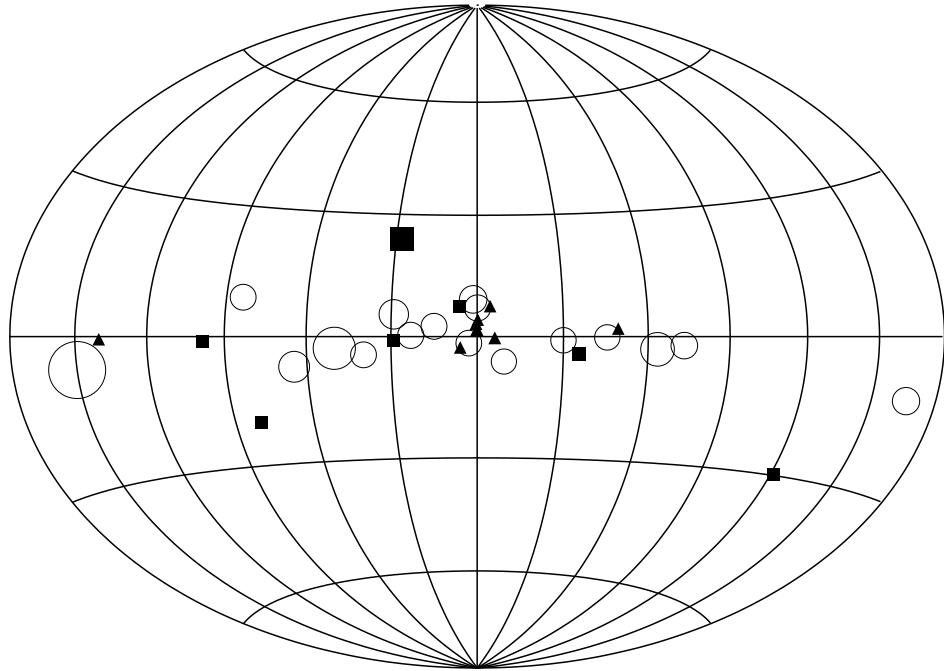


Fig. 26.— Distribution of X-ray nova systems in the Galactic coordinate system. The symbols indicate the type of compact object intrinsic to each system: *empty circles* are for positive and probable BHCs, *filled squares* are for NS, and *filled triangles* are for unknown types. Symbol sizes are proportional to XN peak intensities.

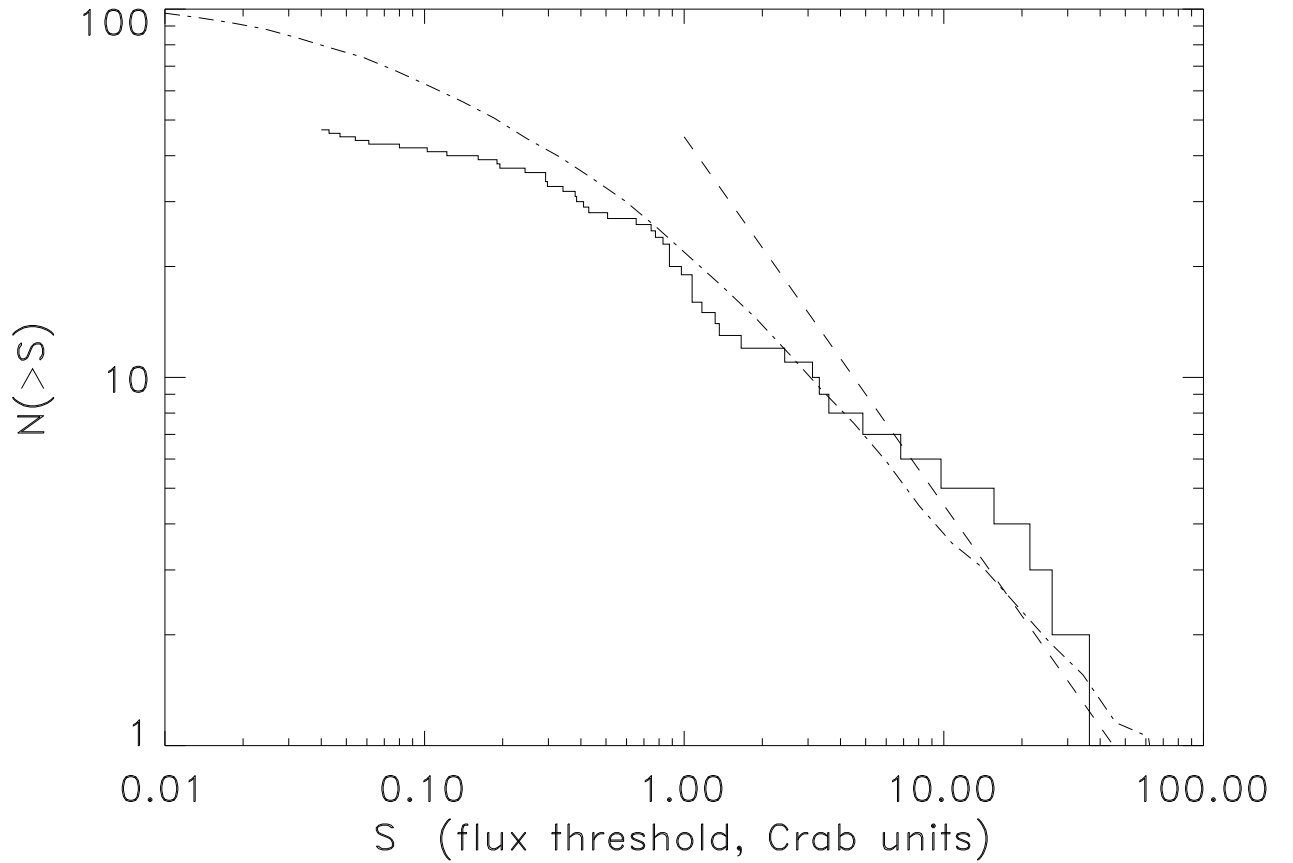


Fig. 27.— The  $\log N - \log S$  distribution (*solid line*) of the peak X-ray fluxes of all the XN outbursts. The *dashed line* is for sources uniformly distributed on a disk of infinite size,  $N \propto S^{-1}$ . The *dot-dashed line* is for a source distribution model on a finite disk of 12 kpc in radius while the observer is at 8.5 kpc from the center (see text).

Table 1. Black Hole X-Ray Nova Systems

Source Name (1)	X-ray Nova Designation (2)	$f_M$ ( $M_\odot$ ) (3)	$i$ (deg) (4)	$M_{\text{BH}}$ ( $M_\odot$ ) (5)	Star Sp (6)	$M_c$ ( $M_\odot$ ) (7)	Ref. (8)
A 0620–00	XN Mon 1975	2.91±0.08	66°±4°	4.9–10	K4 V	0.4–0.7	1–3
H 1705–250	XN Oph 1977	4.0±0.8	70°±10°	4.9±1.3	K3 V	0.7	4–6
GS 2000+25	XN Vul 1988	4.97±0.10	65°±9°	8.5±1.5	K2-K7 V	0.4–0.9	7
GS 2023+338	XN Cyg 1989	6.08±0.06	56°±2°	12.3±0.3	K0 IV	0.9	8–12
GRS 1124–683	XN Mus 1991	3.01±0.15	54°–65°	5.0–7.5	K2 V	0.8	13
GRO J0422+32	XN Per 1992	1.21±0.06	48°±3°	3.57±0.34	M2 V	0.4	14–16
GRO J1655–40	XN Sco 1994	3.16±0.15	69°.5±0°.08	7.02±0.22	F3-F6 IV	1.2–1.5	17

Note. — Col. (3) Mass function; Col. (4) Orbital inclination angle; Col. (5) Mass of the black hole; Col. (6) Spectral type of the secondary star; Col. (7) Mass of the secondary star

References. — (1) McClintock & Remillard 1986; (2) Haswell et al. 1994; (3) Shahbaz, Naylor, & Charles 1994; (4) Remillard et al. 1994; (5) Martin et al. 1995; (6) Remillard et al. 1996; (7) Callanan et al. 1996; (8) Casares, Charles, & Naylor 1992; (9) Wagner et al. 1992; (10) Casares & Charles 1994; (11) Shahbaz et al. 1994; (12) Sanwal et al. 1996; (13) Orosz et al. 1996; (14) Orosz & Bailyn 1995; (15) Casares et al. 1995; (16) Filippenko, Matheson, & Ho 1995; (17) Orosz & Bailyn 1997.

Table 2. X-ray Nova Sources

Source	XN Designation	X-ray Source	Variable Star	Other Name(s)
3U 0042+32				2A 0042+323
GROJ0422+32	XN Per 1992		V518 Per	GRS 0417+335
A 0620–00	XN Mon 1975	Mon X-1	V616 Mon	Nova Mon 1917
EXO 0748–676			UY Vol	2E 0748.4–6737
MX 0836–425				4U 0836–42, GS 0836–429
GRS 1009–45	XN Vel 1993			
GS 1124–683	XN Mus 1991		GU Mus	GRS 1121–68
GS 1354–64	XN Cen 1967	Cen X-2 <sup>a</sup>		MX 1353–644
4U 1456–32	XN Cen 1969	Cen X-4	V822 Cen	2E 1455.2–3127
A 1524–62		TrA X-1	KY TrA	
4U 1543–47				MX 1543–475
4U 1608–522		GX 331–1	QX Nor	1ES 1609–52.2
4U 1630–472		Nor X-1		GX 337+00, A 1630–472
GROJ1655–40	XN Sco 1994			
H 1705–250	XN Oph 1977		V2107 Oph	A 1705–250
GRS 1716–249	XN Oph 1993			GRO J1719–24
4U 1730–220				
A 1742–289		GX .2–.2		A 1743–288
EXO 1846–031				
4U 1908+005		Aql X-1	V1333 Aql	A 1908+005
GRS 1915+105				
4U 1918+146				A 1918+14, H 1922+154
GS 2000+25	XN Vul 1988		QZ Vul	
GS 2023+338	XN Cyg 1989		V404 Cyg	Nova Cyg 1938

<sup>a</sup>Identification of GS 1354–64 with Cen X-2 is uncertain (Kitamoto et al. 1990).

Table 3. Possible X-ray Nova Sources

Source	Other Name(s)	Note
MX0656–072	3A 0656–072	
4U1516–56	Cir X-1, BR Cir	A high-mass system?
A1658–298	V2134 Oph, H 1658–298, MX 1659–29	
4U1659–487	GX 339–4, V821 Ara, A 1659–487	
MX1730–335	Rapid Burster, 4U 1730–333	
KS1731–260	IRAS 17311–2604	
KS1732–273		
GS1734–275		
4U1735–28	GX 359+2, H 1735–285	
X1740–294	GC X-4	Not in SIMBAD database.
GRS1741–288		
KS1741–293	MXB 1743–29	
H1741–322		
X1742–294	GC X-2	Not in SIMBAD database.
A1744–36		
MX1746–203	4U 1743–19, H 1745–203	
EXO1747–214	GPS 1747–212	
A1749–285	GX+1.1,–1.0	Not in SIMBAD database.
MX1803–245		
GS1826–238		



Table 4. General Information of X-Ray Nova Systems<sup>a</sup>

Source	Type <sup>b</sup>	RA (2000)	Dec (2000)	$l$ (deg)	$b$ (deg)	$D$ (kpc)	Star Sp	$m_V$ (mag)	$A_V$ (mag)	$P_{\text{orbit}}$ (day)	Ref.
(1)	(2)	(3)	(4)	(5)	(6)	(7)	(8)	(9)	(10)	(11)	(12)
0042+32	BH?	00 44 50.4	+33 01 17	121.3	-29.8	7?	G?	19.29	0.6	11.6	1,2
J0422+32	BH	04 21 42.75	+32 54 26.8	165.9	-11.9	2.2	M0 V	22.24	1.2	0.212	1,2
0620-00	BH	06 22 44.51	-00 20 44.5	210.0	-6.5	0.87	K4 V	18.4	1.2	0.323	1,2
0748-676	NS	07 48 33.8	-67 45 08.6	280.0	-19.8	2.1		>23	1.26	0.159	1,2
0836-429	NS	08 37 23	-42 53.1	261.9	-1.1	10?		>23	11		1,2
1009-45	BH?	10 11 32	-44 49 41	276.2	+9.0	3?		>21	5		3,12
1124-683	BH	11 26 26.64	-68 40 32.5	295.3	-7.1	5.5	K5 V	20.5	0.87	0.433	1,9
1354-64	BH?	13 58 09.68	-64 44 04.9	310.0	-2.8	10?		22?	3		1,2
1456-32	NS	14 58 22.0	-31 40 07	332.2	+23.9	1.2	K3 V	18.3	0.3	0.629	1,2
1524-62	BH?	15 28 17.1	-61 52 58	320.3	-4.4	4.4		>21	2.4		1,2
1543-47	BH?	15 47 08.5	-47 40 10	330.9	+5.4	4	A2 V?	16.7?	2.1	0.6?	1,2
1608-522	NS	16 12 42.9	-52 25 23	330.9	-0.9	3.3		>20	5.2		1,2
1630-472	BH?	16 34 00.4	-47 23 39	336.9	+0.3	10?			27		1,2
J1655-41	BH	16 54 00.00	-39 50 44.0	345.0	+2.5	3.2	F5-G2	17.3	3.45	2.62	4,5,11
1705-250	BH	17 08 14.5	-25 05 29	358.6	+9.1	4.3	K3 V	21.3	4.5	0.521	1,2
1716-249	BH?	17 19 36.87	-24 01 03.4	0.1	+7.0	2.4		>21	2.4		6
1730-220	NS?	17 33 56.5	-22 02 07	4.5	+5.9						1,2
1742-289	NS	17 45 37.0	-29 01 07	359.9	-0.0	8.5			100		1,2
1846-031	BH?	18 49 17.01	-03 03 43.1	30.0	-0.9	7?			18		1,2
1908+005	NS	19 11 15.95	+00 35 06	35.4	-4.3	2.5	K0 V	19.2	1.2	0.792	1,2
1915+105	BH?	19 15 11.49	+10 56 44.9	45.4	-0.2	12.5		>19	25		7,8
1918+146	BH?	19 20 17	+14 42 19	49.3	+0.4						1,2
2000+25	BH	20 02 49.52	+25 14 11.3	63.4	-3.0	2	K5 V	21.2	5.4	0.344	1,10
2023+338	BH	20 24 03.8	+33 52 04	73.1	-2.1	3.5	K0 IV	19	3.0	6.46	1

<sup>a</sup>Most data are from vP95 which also contains exhaustive references for each source.

<sup>b</sup>We use “BH” or “NS” for firm BH or NS systems, “BH?” or “NS?” for BHC or NS candidates.

References. — (1) van Paradijs 1995; (2) Bradt & McClintock 1983; (3) Bailyn & Orosz 1995; (4) Bailyn et al. 1995; (5) Harmon et al. 1995; (6) Della Valle, Mirabel, & Rodriguez 1994; (7) Mirabel et al. 1994; (8) Mirabel & Rodriguez 1994; (9) Orosz et al. 1996; (10) Callanan et al. 1996; (11) Orosz & Bailyn 1997; (12) Della Valle & Benetti 1993.

Table 5. Morphological Types of X-Ray Light Curves

	Type	Code	Number		Definition
			X-ray	Optical	
1a	FRED	F	14		Fast rise followed by exponential decay.
1b	Possible FRED	F'	6	9	Exponential decay with no rise phase data.
2	Triangle	T	7		Rise timescales $> 1/3$ decay timescale.
3a	Short plateau	Ps	4		Short ( $< 30$ days) flat top.
3b	Long plateau	Pl	4		Long ( $> 30$ days) flat top.
4	Variable decay	V	4		Several decay stages or wiggles.
5	Multiple peak	M	4		Multiple peaks of similar strength.
	Uncertain	U	2	1	Uncertain shape.

Table 6. Quiescent X-Ray Emission

Source (1)	Date (2)	$\Delta$ Mon (3)	S.I/Band (4)	$F_{q,obs}$ (5)	$\log(F_q)$ (6)	$\log(L_q)$ (7)	$\log(\dot{M}_q)$ (8)	Ref. (9)
0042+32	1978?	$\geq 10$	AS?/2-11	$< 0.41$	$< -10.82$	$< 35.03$	$< -10.72$	1
J0422+32	1992/02	-6	RP/0.01-2	$< 0.0088$	$< -13.11$	$< 31.90$	$< -13.86$	9
0620-00	1992/03	+199	RP/0.4-1.4	0.0043	-13.63	30.79	-14.96	2
0748-676	1980/05	-57	EI/0.2-3.5	0.030	-11.94	33.04	-12.72	10
0836-429	1991/05	+244	RP/1-2.4	2.26	-9.46	36.82	-8.93	11
1009-45	1991-?	$\geq 10$	CB/20-100	$< 5$	$< -8.80$	$< 36.69$	$< -9.07$	18
1124-683	1992/03	+14	RP/0.3-2.4	$< 0.0039$	$< -13.12$	$< 32.66$	$< -13.10$	3
1354-64	1975?	$\geq 92$	AS/2-10	3.4	-10.03	36.14	-9.61	1
1456-32	1994/02	+177	A/0.5-4.5	0.070	-11.89	32.46	-13.29	4,13
1524-62	1991/02	+6	RP/0.1-2.4	$< 0.029$	$< -12.24$	$< 33.40$	$< -12.36$	5
1543-47	1990/08	-20	RP/0.4-2.4	$< 0.013$	$< -12.61$	$< 32.88$	$< -12.87$	12
1608-522	1993/08		A/0.5-10	0.0134	-12.49	33.23	-12.53	13
1630-472	1993/03	+6	RP/0.1-2.4	$< 0.0046$	$< -11.11$	$< 35.55$	$< -10.20$	6
J1655-40	1996/03	-2	A/2-10	0.0061	-12.82	32.52	-13.23	14
1705-250	1991/03	+163	RH/0.4-2.4	$< 0.0165$	$< -12.32$	$< 32.88$	$< -12.88$	7
1716-249	1991-94	$> -4$	CB/20-100	$< 5$	$< -9.89$	$< 35.14$	$< -10.61$	15,18
1730-220	1970-74	$> -24$	U/2-6	$< 4.0$	$< -9.94$	$< 35.19$	$< -10.57$	16
1742-289	1974?	$> -2$	AR/3-10	$< 8.66$	$< -9.74$	$< 36.93$	$< -8.82$	1
1846-031	1991-95	$> 20$	CB/20-100	$< 5$	$< -10.57$	$< 35.44$	$< -10.32$	1
1908+005	1992/03	?	RP/0.4-2.4	0.0372	-12.29	32.81	-12.95	7
1915+105	1991-92	$> -4$	CB/20-100	$< 5$	$< -10.12$	$< 36.62$	-9.14	17,18
1918+146	1973?	$> 6$	U/2-10	$< 5.0$	$< -9.76$	$< 35.48$	$< -10.28$	1
2000+25	1992/05	+48	RP/0.4-2.4	$< 0.00036$	$< -13.88$	$< 31.47$	$< -14.28$	7
2023+338	1992/11	+42	RP/0.2-2.4	0.02	-12.49	33.84	-11.91	8

Note. — Col. (2) Observation year/month;  
Col. (3) Months after (+) or before (-) the nearest outburst peak;  
Col. (4) Satellite-Instrument/Band (keV). Satellite-instrument code: A-*ASCA*, AR-*Ariel 5/RMP*, AS-*Ariel 5/SSI*, CB-*Compton/BATSE*, EI-*Einstein/IPC*, RH-*ROSAT/HRI*, RP-*ROSAT/PSPC*, U-*UHURU*;  
Col. (5) Observed quiescent flux or flux upper limit in units of mCrab in the observed band;  
Col. (6) Logarithmic quiescent 0.4-10 keV flux in units of  $\text{ergs s}^{-1} \text{cm}^{-2}$ ;  
Col. (7) Logarithmic quiescent 0.4-10 keV luminosity in units of  $\text{ergs s}^{-1}$ ;  
Col. (8) Logarithmic quiescent mass accretion rate in units of  $M_{\odot} \text{yr}^{-1}$ .

References. — 1. van Paradijs 1995; 2. McClintock, Horne, & Remillard 1995; 3. Greiner et al. 1994; 4. van Paradijs et al. 1987; 5. Barret et al. 1995; 6. Parmar, Angenili, & White 1995; 7. Verbunt et al. 1994; 8. Wagner et al. 1995; 9. Callanan et al. 1996; 10. Parmar et al. 1986; 11. Belloni et al. 1993; 12. Greiner et al. 1994; 13. Asai et al. 1996; 14. Robinson et al. 1996; 15. Harmon & Paciesas 1993; 16. Cominsky et al. 1978; 17. Paciesas et al. 1996; 18. S.N. Zhang, 1997 (private communication).





Table 7—Continued

Source (1)	Outburst yr/mon (2)	X-ray							Optical					Ref. (15)
		Mor. type (3)	S.I./Band (keV) (4)	$F_{p,obs}$ (Crab) (5)	$\log(L_{obs})$ (erg/s) (6)	$\tau_r$ (day) (7)	$\tau_d$ (day) (8)	$T_{obs}$ (day) (9)	Mor. type (10)	$m_{v,p}$ (mag) (11)	$\Delta m_v$ (mag) (12)	$\tau_{d,o}$ (day) (13)	$T_{obs,o}$ (day) (14)	
1915+105	1992/08	Pl	CB/20-100	0.3	37.80	19.5	2370	542						28,49
1918+146	1972/07	F'	U/2-6	0.05	35.94	3.5	8.4	28						63
2000+25	1988/05	F	GA/3-6	12	37.99	0.3	30.1	169	F'	18.1	3.1	102.5	212	50-52
2023+338	1938/10								F'	12.5	6.5	25.2	65	53
	1956/08									14.1				54
	1989/05	F	GL/1.7-37	21	39.31	5.5	38.8	178	F'	17.9	1.1	7.3	36	55-58

Note. — Col. (3) and (9) The light curve morphology types.

Col. (4) Observing satellite/instrument code: AA: *Ariel 5/ASM*; AS: *Ariel 5/SSE*; B: Balloon experiments; C: *Copernicus*; CB: *Compton/BATSE*; E: *Einstein*; EM: *EXOSAT/ME*; GA: *Ginga/ASM*; GL: *Ginga/LAC*; GS: *Granat/Sigma*; GW: *Granat/Watch*; H: *Hakucho*; H1: *HEAO-1*; MH: *Mir-Kvant/HEXE*; MT: *Mir-Kvant/TTM*; O: *OSO-7*; R: Rocket experiments; RP: *Rosat/PSPC*; S: *SAS-3*; T: *Tenma*; VA: *Vela 5A*; VB: *Vela 5B*; U: *UHURU*; XA: *RXTE/ASM*.

References. — (1) Laros & Wheaton 1980; (2) Watson & Ricketts 1978; (3) Paciasas et al. 1995; (4) Callanan et al. 1995; (5) Eachus, Wright, & Liller 1976; (6) Elvis et al. 1975; (7) Kaluziński et al. 1977; (8) Tsunemi et al. 1977; (9) Lloyd, Noble, & Penston 1977; (10) Parmar et al. 1986; (11) Markert et al. 1977; (12) Aoki et al. 1992; (13) Paciasas et al. 1995; (14) Bailyn & Orosz 1995; (15) Kaniovsky et al. 1993; (16) Della Valle et al. 1997; (17) Chodil et al. 1968; (18) Kitamoto et al. 1990; (19) Conner, Evans, & Belian 1969; (20) Evans, Belian, & Conner 1970; (21) Kaluziński et al. 1980; (22) Canizares et al. 1980; (23) Matsuoka et al. 1980; (24) Barret et al. 1992; (25) Matilsky et al. 1972; (26) Li, Sprott, & Clark 1976; (27) Kitamoto et al. 1984; (28) Harmon et al. 1994; (29) Lochner & Roussel-Dupré 1994; (30) Kaluziński & Holt 1975; (31) Kaluziński 1977; (32) Jones et al. 1976; (33) Kaluziński & Holt 1978; (34) Share et al., 1978; (35) Parmar, Stella, & White 1986; (36) Tanaka 1984; (37) Harmon et al. 1995; (38) Bailyn et al. 1995; (39) Watson, Ricketts, & Griffiths 1978; (40) Wilson & Rothschild 1983; (41) Griffiths et al. 1978; (42) Paciasas et al. 1995; (43) Eyles et al. 1975; (44) Branduardi et al. 1976; (45) Parmar et al. 1993; (46) Kaluziński et al. 1977; (47) Thorstensen, Charles, & Bowyer 1978; (48) Charles et al. 1980; (49) Paciasas et al. 1996; (50) Tsunemi et al. 1989; (51) Tanaka, Makino, & Dotani 1991; (52) Chevalier & Ilovaisky 1990; (53) Casares et al. 1991; (54) Richter 1987; (55) Tanaka 1989; (56) Kitamoto et al. 1989; (57) Wagner et al. 1991; (58) Terada et al. 1994; (59) Ebisawa et al. 1994; (60) Kaluziński et al. 1975; (61) Barret et al. 1995; (62) van der Woerd & White 1989; (63) Cominsky et al. 1978; (64) Forman, Jones, & Tananbaum 1976; (65) Mitsuda et al. 1989; (66) Parmar, Angelini, & White 1995; (67) Parmar et al. 1997; (68) in 't Zand 1992; (69) Della Valle et al. 1994; (70) Priedhorsky & Terrell 1984; (71) Czerny, Czerny, & Grindlay 1987; (72) Holt & Kaluziński 1979; (73) Koyama et al. 1981; (74) Kitamoto et al. 1993; (75) Belloni et al. 1993; (76) Zhang et al. 1996; (77) Della Valle, Jarvis, & West 1991; (78) Zhang et al. 1997; (79) Remillard 1997; (80) Cui 1997 (priv. comm.).

Table 8. Energy Output of XN Outbursts

Source (1)	Outburst (2)	$\log(F_p)$ (3)	$\log(L_p)$ (4)	$\log(\frac{L_p}{L_q})$ (5)	$\log(\frac{L_p}{L_{\text{Edd}}})$ (6)
0042+32	1970/02	-9.20	36.60	> 1.57	-2.51
	1977/02	-8.81	36.99	> 1.96	-2.13
J0422+32	1992/08	-7.46	37.29	> 5.39	-1.37
0620-00	1975/08	-6.00	38.09	7.30	-0.87
0748-676	1985/02	-8.85	35.93	2.89	-2.33
0836-429	1971/01	-8.80	37.49	0.67	-1.62
	1990/11	-9.32	36.97	0.15	-2.15
1009-45	1993/09	-7.73	37.55	> 0.86	-1.57
1124-683	1991/01	-6.77	38.86	> 6.21	-0.08
1354-64	1967/04	-6.54	39.58	3.44	0.46
	1971?	-8.97	37.43	1.29	-1.69
	1987/02	-8.54	37.85	1.71	-1.26
1456-32	1969/07	-5.87	38.40	5.94	0.14
	1979/05	-7.11	37.29	4.83	-0.97
1524-62	1974/11	-8.53	37.17	> 3.77	-1.95
	1990/08	-8.60	37.10	> 3.70	-2.02
1543-47	1971/08	-7.24	38.28	> 5.40	-0.83
	1983/08	-6.65	38.85	> 5.97	-0.26
	1992/04	-7.54	37.93	> 5.05	-1.19
1608-522	1970/04	-7.65	37.75	4.52	-0.51
	1970/09	-7.73	37.67	4.44	-0.59
	1971/06	-7.76	37.63	4.40	-0.63
	1971/09	-7.71	37.68	4.45	-0.58
	1975/11	-7.97	37.43	4.20	-0.83
	1977/07	-7.47	37.92	4.69	-0.34
	1979/02	-7.83	37.56	4.33	-0.70
	1979/04	-8.03	37.36	4.13	-0.90
	1983/04	-7.81	37.73	4.50	-0.53
	1991/04	-9.11	36.10	2.87	-2.16
1630-47	1971/02	-8.41	38.46	> 2.91	-0.65
	1972/10	-8.66	38.21	> 2.66	-0.90
	1974/04	-8.21	38.66	> 3.11	-0.45
	1976/06	-8.12	38.75	> 3.20	-0.36
	1977/11	-7.64	39.23	> 3.68	0.11
	1979/03	-9.39	37.92	> 2.37	-1.19
	1984/04	-8.51	38.60	> 3.05	-0.52
	1989/03	-8.32	38.39	> 2.84	-0.72
	1992/09	-9.91	37.20	> 1.65	-1.92
J1655-40	1994/08	-7.35	37.86	5.34	-1.10
	1995/08	-7.45	37.77	5.25	-1.19
	1996/07	-7.16	38.02	5.50	-0.94

Table 8—Continued

Source (1)	Outburst (2)	$\log(F_p)$ (3)	$\log(L_p)$ (4)	$\log(\frac{L_p}{L_q})$ (5)	$\log(\frac{L_p}{L_{\text{Edd}}})$ (6)
1705–250	1977/08	–7.24	38.04	> 5.16	–0.76
1716–249	1993/10	–6.72	38.39	> 3.25	–0.73
1730–220	1972/08	–8.44	36.68	> 1.49	–1.58
1742–289	1975/02	–7.39	39.28	> 2.35	0.16
1846–031	1985/04	–8.07	38.06	> 2.62	–1.06
1908+005	1969/12	–7.64	37.29	4.48	–0.97
	1970/08	–7.94	36.99	4.18	–1.27
	1971/09	–7.62	37.31	4.50	–0.95
	1972/04	–7.86	37.07	4.26	–1.19
	1973/01	–7.64	37.30	4.49	–0.96
	1974/04	–7.33	37.60	4.79	–0.66
	1975/06	–7.56	37.37	4.56	–0.89
	1976/06	–7.67	37.26	4.45	–1.00
	1978/06	–7.50	37.42	4.61	–0.84
	1979/03	–7.85	37.08	4.27	–1.18
	1980/05	–8.78	36.15	3.34	–2.11
	1987/03	–7.20	37.74	4.93	–0.52
	1988/10	–7.59	37.35	4.54	–0.91
1989/09	–7.89	37.05	4.24	–1.21	
1915+105	1992/08	–7.47	39.00	> 2.38	–0.42
1918+146	1972/07	–8.76	36.48	> 1.00	–2.64
2000+25	1988/05	–6.71	38.60	> 7.13	–0.45
2023+338	1989/10	–6.24	39.14	5.30	–0.06

Note. — Col. (3) Calibrated peak flux in 0.4–10 keV band in units of  $\text{ergs s}^{-1} \text{cm}^{-2}$ .

Col. (4) Logarithmic luminosity in 0.4–10 keV band. For unknown distance, we assume 3 kpc.

Col. (5) Logarithmic outburst amplitude (or lower limit) in 0.4–10 keV band as the ratio of the peak luminosity to the quiescent luminosity (or upper limit).

Col. (6) Logarithmic peak 0.4–10 keV luminosity in Eddington units. For unknown masses, we assume  $5M_{\odot}$  for BHCs and  $1.4M_{\odot}$  for NS.



Table 9. Duration and Total Energy

Source	Year	$T_{\text{obs}}$ (day)	$T_{\text{exp}}$ (day)	$T_{\text{r,exp}}$ (day)	$T_{\text{d,exp}}$ (day)	$\log(E)$ (ergs)	$\log(\Delta M)$ ( $M_{\odot}$ )
0042+32	77/02*	58	>17	>4	>12	42.51	–10.74
J0422+32	92/08	228	>517	>16	>501	43.85	–9.40
0620–00	75/08	231	468	26	442	44.47	–8.78
1009–45	93/09	139	>177	>2	>174	44.37	–8.88
1124–683	91/01	261	>417	>12	>404	45.26	–7.99
1354–64	67/04	44	292	126	165	46.08	–7.17
	87/02	199	304	121	182	44.67	–8.58
1456–32	69/07	80	510	5	504	44.91	–8.35
	79/05	33	75	22	53	43.06	–10.19
1524–62	74/11	148	>523	>25	>498	43.88	–9.37
1543–47	71/08	507	>545	>14	>530	44.86	–8.39
	83/08	185	>254	>8	>246	45.06	–8.19
	92/04	9	>26	>8	>18	43.23	–10.03
1608–52	70/09	78	383	227	155	44.18	–9.07
	71/06	42	146	14	132	43.73	–9.52
	71/09	53	272	98	174	44.04	–9.21
	77/07	198	292	28	264	44.29	–8.96
	79/02	37	284	80	203	43.95	–9.30
	79/04	43	220	93	127	43.66	–9.59
1630–47	71/02	93	>698	>418	>280	45.42	–7.83
	72/10	119	>281	>7	>273	44.81	–8.44
	74/04		>762	>78	>683	45.62	–7.63
	76/06 <sup>†</sup>	239	>1067	>109	>957	45.85	–7.40
	77/11	117	>289	>79	>210	45.70	–7.56
J1655–40	94/08*	166	98	35	62	43.70	–9.56
1705–25	77/08 <sup>†</sup>	37	>3983	>5	>3977	44.48	–8.78
1716–25	93/10 <sup>†</sup>		>2905	>5	>2899	45.18	–8.07
1730–22	72/08	230	>344	>61	>282	43.60	–9.65
1742–29	75/02	213	>715	>24	>690	46.23	–7.03
1908+00	71/09	279	325	147	178	43.75	–9.51
	75/06	45	291	44	247	43.76	–9.50
	76/06	53	320	16	304	43.69	–9.56
	78/06	66	252	15	236	43.74	–9.51
1915+10	92/08 <sup>†</sup>	542	>13094	>106	>12987	46.45	–6.80
1918+15	72/07		>27	>8	>19	42.44	–10.81
2000+25	88/05	163	>499	>4	>494	45.02	–8.23
2023+34	89/05	178	590	73	517	45.73	–7.53

\*Observed light curve contains multiple peaks, the expected duration is for only one peak.

<sup>†</sup>Long plateau outburst with cutoff, the expected duration is for an extended plateau phase. The energy fluence is calculated using the observed plateau duration instead of the decay timescale.

Table 10. Outbursts with Plateau

Source	Year	$\tau_{\text{plt}}$ (day)	$T_{\text{plt}}$ (day)	$\tau_{\text{tail}}$ (day)
BHs				
J0422+32	1992	70	15	42
1354–64	1987	360*	57	44
1543–47	1971	540	52	47
1705–250	1977	335*	31	?
1716–249	1993	387	72	1.4
1915+105	1992	2370*	310	20
	Mean	677	90	31
NSs				
1456–32	1979	78	9	3.6
1608–52	1977	860 <sup>†</sup>	51	37
	1979	250 <sup>†</sup>	18	12
1908+005	1975	71*	20	14
	1976	150*	16	21
	1978	110*	15	28
	Mean	258	22	19

\*Flux is highly variable,  $\tau_{\text{plt}}$  is for the overall shape.

<sup>†</sup>This value is highly uncertain due to sparse data.

Table 11. X-ray Nova related X-ray Missions\*

Observatory	Start Year	Stop Year	Coverage factor	FOV	Energy Band
Sounding Rockets	1960's	1960's	$\ll 1$	vary	3–12
Vela	1969.4	1979.6	0.80	$4\pi$	3–12
Ariel-5	1974.9	1980.3	0.90	$4\pi$	3–6
SAS-3	1975.4	1979.5	0.60	$3 \times (1^\circ \times 32^\circ)$	1.5–60
Tenma	1983.5	1984.5	0.90	$45^\circ$	1–60
Hakucho	1979.2	1984.2	0.45	$50^\circ \times 360^\circ$	1.5–30
Ginga	1987.1	1991.8	0.90	$4\pi$	1–20
GRANAT/Watch	1989.9	1992.8	0.80	$3^\circ \times 60^\circ$	6–180
CGRO/BATSE	1991.3	1995.9	0.90	$4\pi$	20–300
Eureka/Watch	1992.8	1993.5	0.10	$60^\circ$	6–180
OSO 3/Copernicus	1967.2	1982.3	0.05	$40^\circ$	8–210
OSO 4	1969.1	1975.6	0.30	$40^\circ \times 360^\circ$	14–200
OSO 5	1972.2	1980.8	0.40	$2 \times (23^\circ \times 360^\circ)$	8–200
EXOSAT	1983.5	1986.3	0.05	$0.8^\circ \times 0.8^\circ$	1–20
HEAO-1	1977.5	1989.5	0.08	$8^\circ \times 360^\circ$	0.2–60
Uhuru	1970.9	1973.3	0.15	$12.7^\circ \times 360^\circ$	2–20

\*All of this information was retrieved from the online database at HEARSAC.

Table 12. Mass Transfer Rate from the Companion

Source	yr/mon	$T_{\text{rec}}$ (yr)	$\log(\dot{M}_{\text{c}})$ ( $M_{\odot}/\text{yr}$ )	$\log(\dot{M}_{\text{c,K}})^*$ ( $M_{\odot}/\text{yr}$ )
0042+32	77/02	7.00	-11.59	
0620-00	75/08	57.75	-10.54	-10.08
1354-64	71/12	4.67	-9.25	
1456-32	79/05	9.83	-11.18	-9.81
1543-47	83/08	12.00	-9.27	
	92/04	8.67	-10.97	
1608-52	70/09	0.42	-8.69	
	71/06	0.75	-9.40	
	71/09	0.25	-8.61	
	77/07	1.67	-9.18	
	79/02	1.58	-9.50	
1630-47	72/10	1.67	-8.66	
	74/04	1.50	-7.81	
	76/06	2.17	-7.74	
	77/11	1.42	-7.71	
1908+00	71/09	1.08	-9.54	-9.56
	75/06	1.17	-9.57	
	76/06	1.00	-9.56	
	78/06	2.00	-9.81	
2023+34	89/05	32.75	-9.05	-8.71

\*Theoretical mass transfer rate from the companion according to King et al. (1996).